

A modelling-based approach to the geothermal energy potential of Svalbard, Norway

Matthijs Nuus

Bachelor Thesis Earth Science, July 2020, 15ects



The Jotunkjeldene hot springs in Bockfjorden, Svalbard (Sund, 2008)

Supervisors:

Dr. H. Paulssen, Utrecht University

Dr. K. Senger, University Centre in Svalbard

P. Betlem PhD candidate University Centre in Svalbard

Table of contents

Acknowledgements	2
Abstract	3
1. Introduction	4
2. Theoretical background	6
2.1 <i>Geothermal gradient and material properties</i>	6
2.1.1 Thermal conductivity	6
2.1.2 Radioactive heat production.....	7
2.2 <i>The heat equation</i>	7
2.3 <i>FiPy background</i>	7
2.4 <i>Geothermal energy systems</i>	8
2.5 <i>Geological background</i>	9
3. Methods and data	12
3.1 <i>Heat Flow Model Improvements</i>	12
3.2 <i>Data Implementation</i>	13
3.3 <i>Implementing and checking the heat fluxes</i>	15
3.4 <i>Adding new boreholes</i>	15
3.4.1 Modelled borehole locations and history	15
3.4.2. Digitizing logged boreholes	16
4. Results	17
4.1 <i>Initial Model Results</i>	17
4.1.1. Model results DH4.....	17
4.1.2 Model results Tromsøbreen-II	20
4.1.3 Model results Grønfjorden-I	23
4.1.4 Model results Sysselembreen.....	24
4.2 <i>Adjusted model parameters</i>	26
5. Discussion	28
5.1 <i>Model outcomes and constraints</i>	28
5.1.1 DH4	28
5.1.2 Tromsøbreen-II	29
5.1.3 Grønfjorden-I	30
5.1.4 Sysselembreen	30
5.3 <i>Geological link to geothermal trends</i>	31
5.4 <i>Geothermal energy on Svalbard and future work</i>	33
6. Conclusions	34
7. References	36

Acknowledgements

I would like to thank Peter Betlem and Kim Senger from the University Centre in Svalbard for giving me the possibility to write my thesis under their supervision. I am grateful for your helpfulness and presence during my work.

A thanks to Hanneke Paulssen from Utrecht University for being my home university supervisor. You gave me the freedom to extent my thesis which made me become more skillful in modelling.

Thanks to the UNIS CO₂ Lab, Norwegian Petroleum Directorate, Norsk Polar Navigasjon, Norwegian Polar Institute and Kirsti Midttømme for data access. Thanks to Jonathan Guyer and the FiPy GitHub community for answering my modelling questions.

Lastly a big thanks to my friends Armin Dachauer, Lise Nakken, Karoline Løvlie, Julian Janocha, Tom Birchall and Gareth Lord for your always entertaining and supporting presence in a due to COVID-19 almost desolated university centre.

Abstract

In this thesis information contributing to a geothermal energy potential assessment is presented. Currently, all settlements on the Arctic Archipelago of Svalbard are powered using fossil-fuel based energy sources. As this region has been undergoing an amplified effect of climate change, finding a renewable and alternative energy source is of high importance. Previous research has shown Svalbard's heat flow values are anomalously higher than those found on the mainland, due to a locally thinned lithosphere. This gives motivation to investigate Svalbard's geothermal energy potential.

By creating a 1D-heat flow model using a FiPy-based Python model, heat flow values for different boreholes across Svalbard were found, as well as the temperature versus depth development. Digitized borehole data and previously measured geophysical parameters of different lithologies were used as input for the model, outputting a temperature curve.

The three of the four boreholes that were investigated confirmed a higher heat flow value compared to mainland Norway ($>70\text{mW/m}^2$). The highest heat flow value found in this thesis was of 91mW/m^2 and found in southern Spitsbergen. The temperature curves showed the importance of geophysical parameters and local geology, as intervals with a higher shale content had a higher geothermal gradient compared to limestone- or sandstone intervals. A possible link between a fault network and convective heat transfer was hypothesized to explain the anomalous heat flow value found at Tromsøbreen-II (7617/1-2) in southern Spitsbergen.

This thesis has shown the possibilities of Python based models to contribute to a study on the geothermal potential of Svalbard. However, more detailed geological knowledge regarding a possible geothermal reservoir is required for a further assessment this study.

1. Introduction

Since the end of the Little Ice Age in 1910, the annual temperature on the High-Arctic archipelago of Svalbard has risen by approximately 4°C (Rachlewicz et al., 2007). Models and empirical evidence have shown the Arctic is especially sensitive to climate change (Svendsen and Mangerud, 1997), a phenomenon called Arctic amplification. This has caused a worldwide debate regarding energy consumption, greenhouse gas releases and protection of vulnerable Arctic areas. As of yet, all settlements on the archipelago are fully dependent on a fossil fuel-based energy supply.

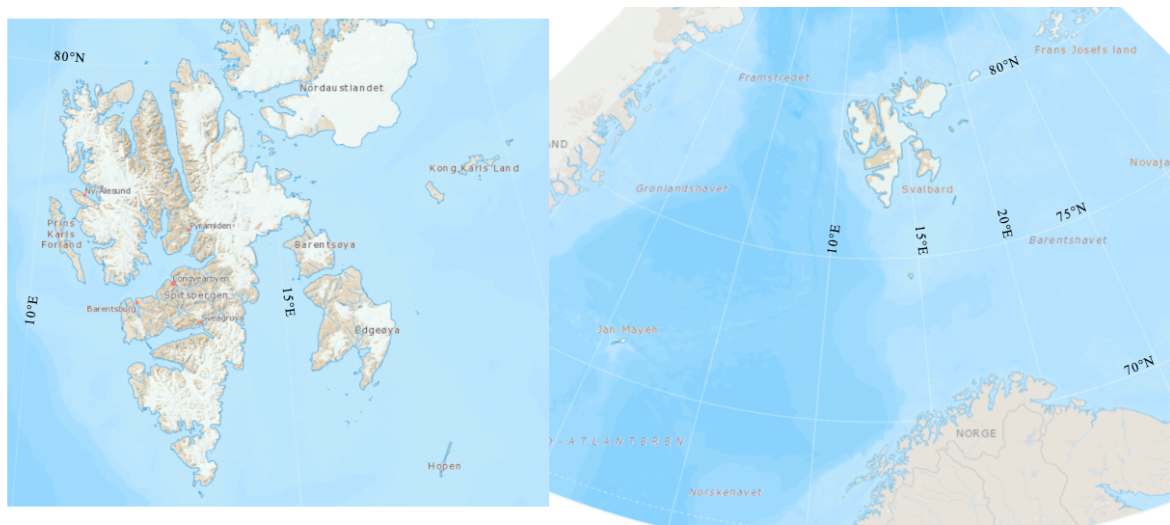


Fig. 1 Location of Svalbard and settlements found on Svalbard. (Polarinstitutt, 2015)

The town of Longyearbyen, situated at 78° north in Nordenskiöldland, Svalbard, (fig. 1) was founded by Americans Frederick Ayer and John Munroe Longyear in 1906 for its abundance in workable and accessible coal. Ten years later it was purchased by the Norwegian coal mining company “Store Norske Spitsbergen Kulkompani A/S”. Several mines have been active since the city was founded, however only one mine is currently still operational (Dallmann et al., 2015). Longyearbyen currently has a population of around 2300 (Olsen et al., 2020)

Besides Longyearbyen, Svalbard counts four more settlements. Barentsburg and Pyramiden are Russian settlements, owned by the coal mining company “Trust Artikulogol”. Barentsburg counts a population of approximately 450 inhabitants and Pyramiden only hosts a few seasonal workers (Gerlach and Kinossian, 2016). Ny-Ålesund, originally founded for its coal, is currently a multinational research station. It has a population of around 30 in winter and 150 in summer, which are all connected to research activities (Shears et al., 1998). Svea is a former Norwegian coal mining settlement disassembled in 2018-present day after the mine “Lunckefjell” closed (Hagen et al., 2018).

The electricity and heat supply of all settlements is dependent on fossil fuel-based energy generation. Longyearbyen and Barentsburg are primarily powered by coal-fuelled power plants (with diesel aggregates as routinely used back-up solutions), while Pyramiden, Ny-Ålesund and Svea all use diesel generators (Krzyszowska, 1985, Weinbruch et al., 2015, Iversen, 2013) .

The emissions from the Longyearbyen powerplant alone resulted in a release of over 60 000 tons in CO₂ in 2014 (SSB.no). Combining this number with additional CO₂ producing factors, Svalbard, if counted as a country, emits more CO₂ per capita than the most emitting country Qatar (ourworldindata.org). This increasing concentration of CO₂ in the atmosphere caused by burning fossil fuels is suggested to enhance the natural greenhouse effect and global warming (Anderson et al., 2016). Direct pollution emissions by the local powerplants additionally have a potential negative impact both on the local Arctic ecosystems and on the local population (Weinbruch et al., 2015)

In a region more vulnerable to climate change, alternative and renewable energy sources for the town should be considered, in order to play a leading role in showing the current Arctic warming crisis. Several projects based on Svalbard have been putting work into finding alternative resources to supply the town with energy or reducing the CO₂ emission. Examples for alternative and renewable energy sources include solar- and wind energy (Buonsanti, 2011), CO₂ capture and -storage (Senger et al., 2015), locally produced natural gas (Ohm et al., 2019) and geothermal energy (Midttømme et al., 2013).

Compared to other types of energy resources, geothermal energy has a low environmental impact (Kristmannsdóttir and Ármannsson, 2003) and is not dependent on weather factors such as wind and sun (Iversen, 2013).

Petroleum exploration borehole data around Svalbard suggests there are geothermal anomalies present, with values as high as 43-52°C/km in southern Spitsbergen (Betlem, 2018). Furthermore, numerous hot springs are present in Svalbard. Temperatures as high as 130–180°C corresponding to depths of 1.6 – 2.3 km are suggested by geothermometers at Troll hot spring in northern Svalbard (Våagnes and Amundsen, 1993). The location of the hot spring is along a fault zone which potentially hosts more hot fluid pathways (Banks et al., 1998). Proximate volcanic centers lie on the same fault zone as the hot springs, the volcanoes may have been active during the last interstadial (Skjelkvåle et al., 1989). It is therefore worthwhile to further investigate the geothermal potential of Svalbard to assess if it can be an alternative energy source for Longyearbyen.

This thesis aims to provide further insights into the possible geothermal potential of Svalbard by creating heat flow- and temperature evolution models using Python. The model creates space for easy adaptation of the data input and allowing for value feedback to find suitable heat flow values for the different boreholes which will be investigated. These values and the resulting temperature versus depth graph will function as a supplement into more detailed knowledge of the lateral distribution of geothermal gradients and heat flow values on Svalbard.

2. Theoretical background

2.1 Geothermal gradient and material properties

The Earth's inner core boundary temperature is estimated to be, at the high end, between 5600 and 6000K (Ma et al., 2004). Decaying radioactive elements, gravitational pressures acting on rocks and minerals and pre-existing heat from when the planet was formed and accreted have caused this generated heat (Omer, 2008). As conduction and convection cause materials to pass on their heat by molecular energy transfer, heat will tend to flow from the warmer core to the colder mantle creating a geothermal gradient. Earth's geothermal gradient is on average 30°C/km (Barbier, 2002) and is calculated by taking the derivative of the temperature versus depth profile (fig. 2).

Different lithologies may possess different geophysical properties that can influence the geothermal gradient. These material properties include density, heat capacity thermal conductivity and radioactive heat production. The latter two are thought to have the most influence on the temperature curve (Henne et al., 2014).

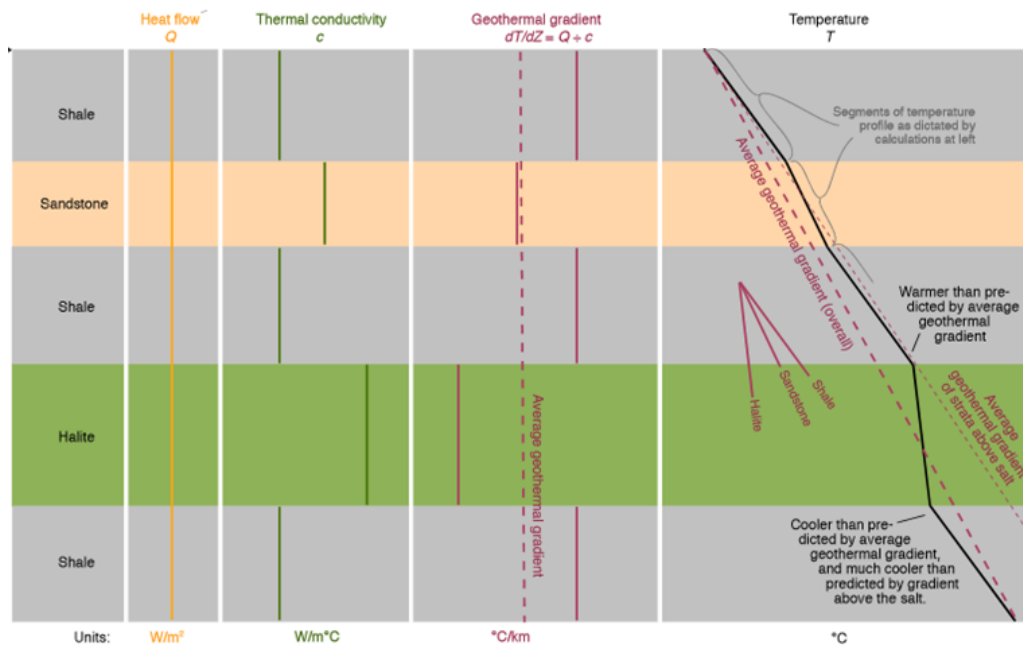


Fig.2 Relationship thermal conductivity versus geothermal gradient. Railsback (2011)

2.1.1 Thermal conductivity

Thermal conductivity describes how well a material conducts heat. A lower thermal conductivity results in a higher geothermal gradient (fig. 2) when a constant heat flux is applied following Fourier's law for heat flow (eq. 2.1).

$$Q = c \frac{dT}{dz} \quad (2.1)$$

In equation 2.1: Q equals the heat flow, c the thermal conductivity and dT/dz the geothermal gradient. Thermal conductivity in rocks depends on factors such as mineral composition, compaction and anisotropy (Labus and Labus, 2017). Quartz content plays an important role in conductivity. Sandstone therefore generally has a higher thermal conductivity than shale

($2.50 - 4.20 \text{ Wm}^{-1}\text{K}^{-1}$ versus $1.05 - 1.45 \text{ Wm}^{-1}\text{K}^{-1}$) (Schön, 2015). Felsic igneous rocks and salts have higher a thermal conductivity than siliciclastic rocks (Labus and Labus, 2017, Zhuo et al., 2016)

2.1.2 Radioactive heat production

Internal radioactive heat production can significantly influence the geothermal gradient (Yuan et al., 2009). A relationship was found between total carbon content and uranium concentration, suggesting a higher radioactive heat production in more organic rich layers (Lüning and Kolonic, 2003). Generally speaking, weakly radioactive rocks include coal, chert, limestone and pure sandstone, while shales and silt are more radioactive (Russell, 1942). This can be partially explained by large openings in the crystal structure of the clay minerals, in which multiple radioactive elements fit well into (Hurley, 2009).

2.2 The heat equation

Geophysical material properties discussed in section 2.4 are the parameters required for the heat equation. This formula allows for the calculation of the incoming heat flux from the Earth's core at a certain depth. The heat equation, which is a special form of the diffusion equation (eq. 2.2), forms the basis of the Svalbard heat flow model.

$$\frac{\partial \phi}{\partial t} = D \nabla^2 \phi \quad (2.2)$$

In equation 2.2, ϕ equals the diffusivity, D the diffusion coefficient and ∇^2 is the Laplacian operator.

For a 1D uniform heat flow scenario, which is the case for a single borehole, the equation can be rewritten into:

$$\frac{\partial u}{\partial t} = \frac{k}{c \rho} \frac{\partial^2 u}{\partial x^2} \quad (2.3)$$

In which u is the temperature, k is the thermal conductivity, c is the specific heat capacity and ρ the density. The diffusivity is here replaced by temperature, and the diffusion coefficient is split into its components. The second term in equation 2.3 ($k/c\rho$), is often referred to as α .

2.3 FiPy background

FiPy is a numerical partial differential equation (PDE) solver that works with Python. It uses the finite volume method to reduce equations within the model to a form manageable to linear solvers (Guyer et al., 2009).

A PDE in the form of equation 2.4 can be solved using FiPy.

$$\frac{\partial(\rho\phi)}{\partial t} - [\nabla \cdot (\Gamma_i \nabla)]^n \phi - \nabla \cdot (\mathbf{u}\phi) - S_\phi = 0 \quad (2.4)$$

The equation is split up into four terms: `TransientTerm(1)`, `DiffusionTerm(2)`, `ConvectionTerm(3)` and the `SourceTerm(4)`. The `Term` is one of three fundamental Python classes used in FiPy (Guyer et al., 2009).

The `TransientTerm` represents the time rate change of the temperature, the `DiffusionTerm` represents the tendency of nonuniformities in the temperature to flatten out and the `SourceTerm` represents any source or sink that injects or removes heat at a specific point (Guyer et al., 2009). The `ConvectionTerm`, representing the “blowing” of the temperature in a velocity field \mathbf{u} (eq. 2.4), will be disregarded in the model (eq. 2.5) as liquid- and gas content of the borehole data are scarce or unavailable.

Using FiPy, numerically solving the heat equation is not necessary. In FiPy one can simply write the collection of desired terms in an equation form, which for the heat flow model case would look like equation 2.5:

$$\text{TransientTerm}() == \text{DiffusionTerm}(D) + \text{SourceTerm}() \quad (2.5)$$

Alongside the `Term` class, two more fundamental Python classes are of importance in FiPy and thus within the to be created heat flow model, namely: `Mesh` and `Variable`.

A `Mesh` object represents the domain of interest. In the case for the heat flow model, this domain would be equivalent to the borehole depth, or the depth to where one wants to model the temperature. The `Variable` object acts as a changeable quantity or field during the PDE-evolution (Guyer et al., 2009). This object is represented by the diffusion coefficient variables (thermal conductivity, density and specific heat capacity), as well as the temperature itself and the radioactive heat production values.

2.4 Geothermal energy systems

Geothermal energy systems make use of the geothermal gradient by extracting thermal energy of Earth’s interior (Huenges and Ledru, 2011). A difference in two types of geothermal systems can be made: high- and low enthalpy systems, depending on what fluid temperature is reached (Barbier, 2002).

In a high enthalpy system, high enough temperatures are reached to produce electricity. A fluid is pumped down into a deep geothermal reservoir and pumped back up again with the demanded temperature (fig. 3a). Three principal factors are required for high enthalpy systems: high enough subsurface temperatures, hot water bearing geologic formations and a sufficient transmissivity of the reservoir rock (Hirschberg et al., 2014). When a hydrothermal resource is unavailable, Enhanced Geothermal Systems (EGS) can be used. In an EGS, cold water is injected in the hot subsurface where rock has been fractured providing a large heat exchange (fig. 3B) (Hirschberg et al., 2014). The hot water or steam then enters turbines generating electricity.

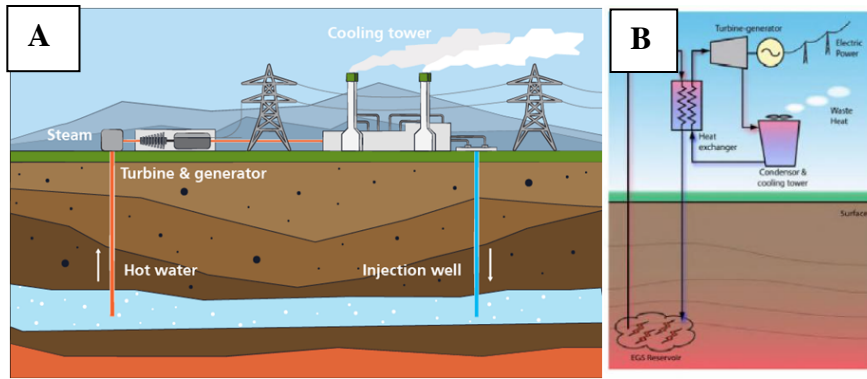


Fig.3 High enthalpy geothermal systems. A: regular deep geothermal plant. B: EGS (Hirschberg et al., 2014)

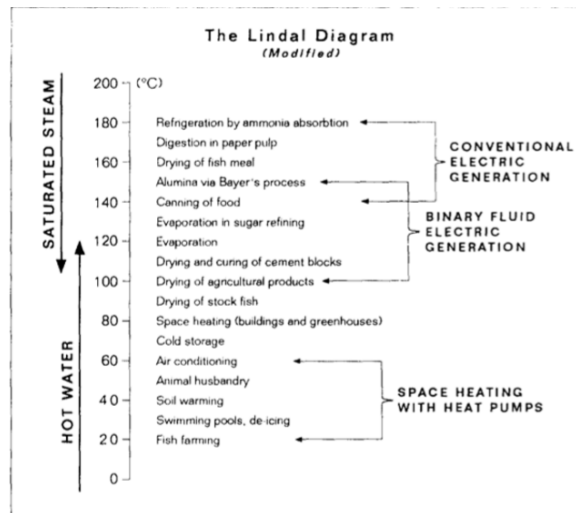


Fig.4 Lindal Diagram of geothermal applications (Lindal, 1973)

Low enthalpy systems are used in shallower dimensions. They do not generate electricity but are rather used for heating purposes (Sanner et al., 2011). An overview of usages of both types of geothermal energy systems is shown in the Lindal Diagram (fig. 4).

2.5 Geological background

Sufficient geological knowledge is necessary for understanding geothermal regimes as a high number of geological features play key roles in a lateral difference of geothermal gradients. Different rock formations possess different geophysical properties that may influence the temperature curve (Henne et al., 2014). Fault- and fracture networks may create fluid pathways of which some have created local geothermal hotspots (fig. 5) (Banks et al., 1998). Knowledge of crustal age is relevant as it thickens and cools down, higher heat flow values can be found close to newly formed crust (Sclater et al., 1980) and geothermal lows are found in cratons (Jones, 1992).

Svalbard's geological history begins with the oldest dated minerals found in metamorphic and igneous rocks from the Late Archean (Dallmann et al., 2015). Up until the Early Paleozoic, metamorphic rocks can be found. These rocks form the crystalline basement of Svalbard (Dallmann et al., 2015)

Rift troughs and -basins dominate the depositional environments in the Late-Devonian up until the Carboniferous. Crustal extension created these basins along pre-existing fault zone, with a North South orientating trend (Dallmann et al., 2015).

A carbonate platform developed in the Permian and is overlain by Mesozoic open-marine deposits (Braathen et al., 2012). Mesozoic reservoir-caprock successions can be found in the vicinity of Longyearbyen. The siliciclastic reservoir units are of Late Triassic to Mid Jurassic age (Ogata et al., 2014a). The reservoir is capped by a shale-dominated succession of Middle to Upper Jurassic age and a succession of Early Cretaceous age (Ogata et al., 2014a). Igneous rocks from the Early Cretaceous are related to the High Arctic Large Igneous Province (HALIP) which developed during the opening of the American basin (Dallmann et al., 2015). Continuous plate motion lead to the formation of the Eurekan Fold Belt, which in Svalbard is known as the West Spitsbergen Fold and Thrust Belt (WSFTB). As a result of this orogeny, the Central Tertiary Basin (CTB) was formed (Dallmann et al., 2015).

Through the Neogene and Quaternary, repeated volcanic activity occurred related to the presence of a hot spot at the Yermak Plateau, north of Svalbard.



Fig.5 Location of geothermal hotspots on Svalbard (Dallmann et al., 2015).

Longyearbyen is located within the Central Tertiary Basin and surrounded by outcropping Early Cretaceous and Paleogene deposits. Moving westwards, the strata get thin-skinned until the WSFTB dominates the outcropping geology. To the east of Longyearbyen lies the Billefjorden Fault Zone, which main phase was last active during the Carboniferous when it functioned as a rift basin (fig. 6C). Most of the documented exploration- and scientific boreholes also lie within the CTB (Senger et al., 2019). A geological overview map, including major fault zones and geological stages is shown in fig.6.

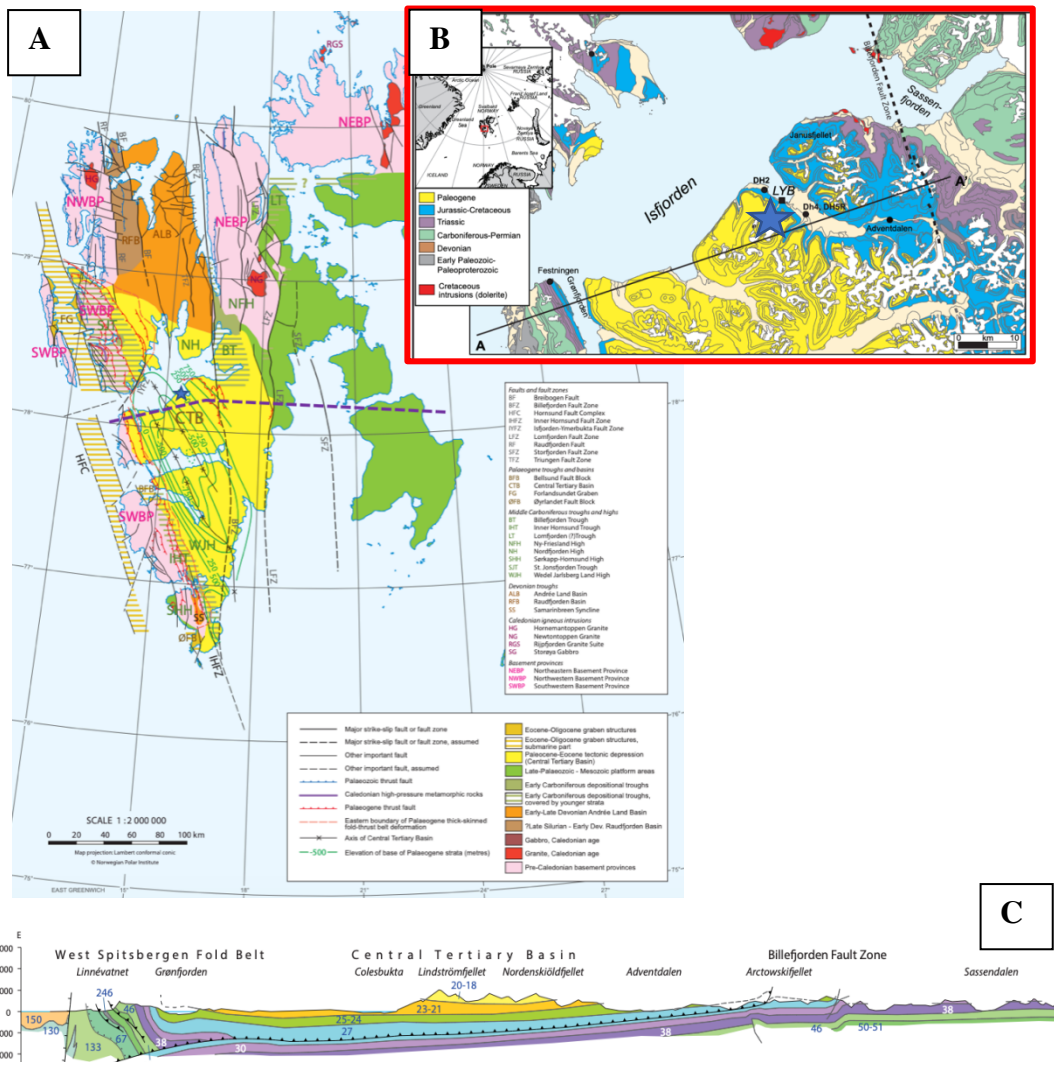


Fig.6. A: Geological overview map of Svalbard (Dallmann, 2015). B: Geology around Longyearbyen (Olaussen et al., 2019). C: cross section along purple dashed line (Dallmann et al. (2015))

3. Methods and data

3.1 Heat Flow Model Improvements

The heat flow model was created using an advanced adaptation of a 1D diffusion problem example provided by FiPy (appendix 1). The example begins with setting up a simple scenario in which the boundary conditions are fixed and there is a uniform diffusivity (fig. 7a-b). In the case for a heat flow model, this means a fixed top- and bottom temperature, alongside uniform geophysical properties of the borehole material.

A constant surface temperature is constrained, alongside a set bottom hole temperature using:

$$\begin{aligned} T.\text{constrain}(\text{valueRight}, \text{mesh.facesRight}) \\ T.\text{constrain}(\text{valueLeft}, \text{mesh.facesLeft}) \end{aligned} \quad (3.1)$$

`valueRight` and `valueLeft`, representing base- and surface temperature, can be chosen randomly but in the first attempt were set to 1 and 0 respectively. The diffusion coefficient D (eq 2.5), which is equal to the second term in equation 2.3, is also set to a value of 1. Equation 1.4 is then solved with the above-mentioned variables.

From this basic set-up (fig. 7a-b), the first simple improvements could be made. These improvements are essential for further work on the model when real data will be applied. The first improvement that was made was a varying surface temperature (fig. 7d). Using a while-loop that kept track of the time within the model, a situation similar to fig.7d was implemented.

The second general improvement that had to be made was implementing a varying lithology in the borehole (fig. 7h). This was done with `if/elif/else`-loops that assigned different geophysical properties to the varying lithology over depth using `.setValue`.

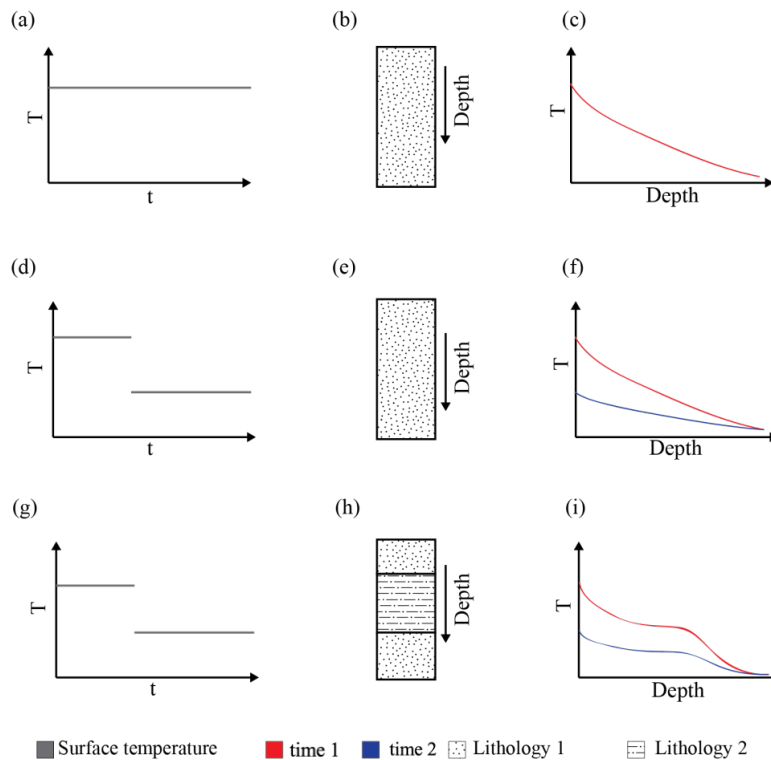


Fig.7 Illustrative image of model improvement. A-C: constant surface temperature, uniform lithology. D-F: varying surface temperature, uniform lithology. G-I: varying surface temperature and lithological variation. C, F, I: depiction of T vs. Depth evolution over time.

3.2 Data Implementation

As the basic model improvements are done, real borehole and historical surface temperature data can be implemented in the model. The data used in the model comes from the CMR-report, an unpublished geothermal pilot project set up by *Store Norske Kulkompani* (Henne et al., 2014). It contains assumed historical surface temperature data as well as material parameters and generalized borehole data for two different boreholes. The first dataset that was implemented was of the DH4 borehole. This borehole is located in Adventdalen, a valley adjacent to Longyearbyen (fig. 8). The borehole was drilled to investigate a potential reservoir for CO₂ sequestration (Ogata et al., 2014b).

Before the data can be correctly implemented, the mesh has to match that of the borehole. All boreholes (section 3.4) were of different depths but were all modelled until a depth of 6000m. The borehole data therefore has to be extrapolated by assuming the lithology and geophysical parameters below the borehole (fig. 10a, b). Taking cells the size of 1m each, the mesh therefore becomes 6000 cells big.

The time over which the model runs is set to 800000 years and the starting temperature at the base of the model equals 180°C. Long term models are insensitive of the initial temperature distribution, but a gradient closer to the final solution has been shown to converge faster (Henne et al., 2014). For all further model adaptations, this same linear starting gradient will therefore be used.

These bigger data sets were dealt with using pandas, which is a Python library containing rich data structures and tools for working with large data sets (McKinney, 2011). Historical surface temperature data (fig. 9) were stored into a pandas.dataframe. The data frame is then looped-over using a while-loop. Using equation 3.1. the surface temperature value was locked for the given time at the top of the mesh.

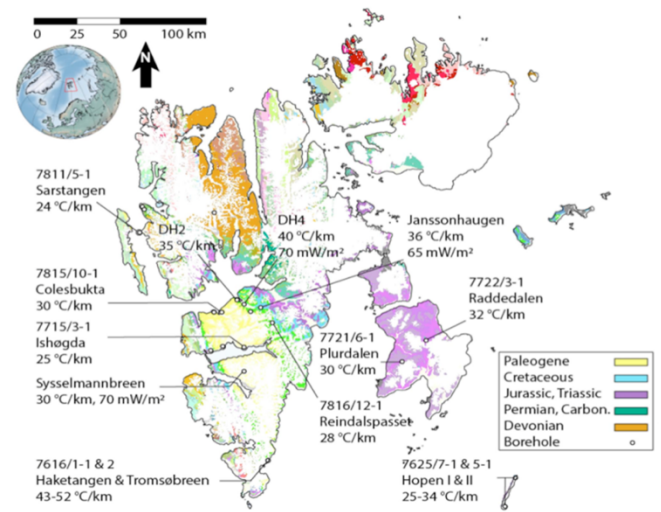


Fig.8 Research and exploration borehole locations on geological map Svalbard (Betlem, 2018)

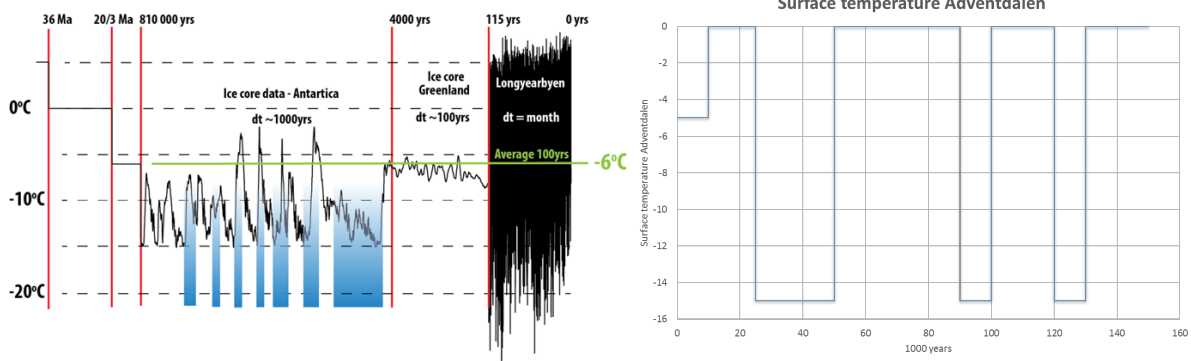


Fig.9 Surface temperature over a period of 36Ma years (left), assumed surface temperature Adventdalen used for simulation (right). Henne et al. (2014).

A second pandas.dataframe was created storing the generalized lithological variations (fig. 10a, b). It was looped over in the same way as when the adaptation in fig.7h was implemented. The material parameters for the individual layers (fig. 11) are based on core samples for the upper 1000m and reflection seismology for the layers below (Henne et al., 2014).

The radioactive heat produced by the different layers were stored into a CellVariable that was then explicitly added to the equation.

One important notice that has to be accounted for, is that the following material parameters contain the unit Watt: thermal conductivity and radioactive heat production. As Watt is a time dependent unit (J/s), it will have to be adjusted the for size of the time step. In the first run the time step will be 100 years. The conversion is as follows: $1W = 1 \frac{J}{s} \approx 3 \times 10^9 \frac{J}{100yr}$

A										
Age Mill year	Geological Time		Depth		Type of rock	Comments	Thermal	Heat	Rock	Radioactive
			From (m)	To (m)			conductivity k - W/mK	Capacity J/kg·K	Density kg/m ³	Heat prod μW/m ³
65-175	Jurassic- Cretaceous	Bed 1	0	190	Sandstone	Permafrost	3,0	850	2200	1
		Bed 2	190	540	Shale /siltstone		2,0	850	2400	1,5
		Bed 3	540	590	Sandstone		3,0	850	2200	1
		Bed 4	590	670	Shale/siltstone		2,0	850	2400	1,5
175-250	Triassic - Jurassic	Bed 5	670	700	Sandstone		3,0	850	2200	1
		Bed 6	700	770	Shale /siltstone		2,0	850	2400	1,5
		Bed 7	770	800	Sandstone		3,0	850	2200	1
		Bed 8	800	1200	Shale /siltstone		2,0	850	2400	1,5
		Bed 9	1200	1230	Igneous intrusion		2,0	850	2700	1,5
		Bed 10	1230	1500	Shale		2,0	850	2600	1,5
250-360	C-P	Bed 11	1500	2000			3,0	850	2200	1
360-415	Devonian		2000	6000			3,0	850	2200	1

B										
Age Mill year	Geological Time		Depth		Type of rock	Thermal	Heat	Rock	Radioactive	
			From (m)	To (m)		conductivity k - W/mK	Capacity J/kg·K	Density kg/m ³	Heat prod μW/m ³	
37- 58	Eocene	Aspelintoppen Fm	0	90	Mix	2,5	850	2500	1	
		Battfjellet Fm	90	180	Mix	2,5	850	2500	1	
		Frysaodden Fm	180	330	Shale	2,2	850	2600	1,5	
		Bjørnsonfjellet Fm	330	430	Sandstone	4,5	850	2200	1	
		Frysaodden Fm	430	770	Shale	2	850	2600	1,5	
58-67	Paleocene	Grumantbyen Fm	770	920	Sandstone	3,3	850	2200	1	
		Basilika Fm	920	1040	Shale	2,1	850	2600	1,5	
?	?	Basement ?	1040	6000	Basement	3	850	2200	1,5	

Fig.10a,b: Generalized borehole data and material parameters for DH4 and Sysselembreen. Henne et al. (2014)

3.3 Implementing and checking the heat fluxes

Currently the model has a fixed bottom hole temperature. However, the bottom hole temperature of the model is unknown and changes over time. Therefore, instead of using a fixed temperature value, a constant heat flux is supplied from the base of the model. This can simply be changing `valueRight` to `fluxRight` and constraining it in using:

$$T.\text{faceGrad.constrain}([\text{fluxRight}], \text{mesh.facesRight}) \quad (3.2)$$

The heat flow values for DH4 range from 60-80mW/m² (Henne et al., 2014). In order to check which heat flux value is most accurate, the root mean square error (eq. 3.3) of the plotted graph versus the real temperature curve is calculated. The real time temperature curve was provided by Kirsti Midtømme and contained temperature measurements on centimeter scale. These were converted into meter scale for more easy comparison with the plotted model.

$$RMS_{Error} = \sqrt{\frac{\sum_{i=1}^n (\hat{y}_i - y_i)^2}{n}} \quad (3.3)$$

The \hat{y}_i -value in equation 3.3 represents the temperature value for every Cell in the Mesh of the plotted temperature model. The y_i -value represents the temperature value of the real time temperature curve.

After the first run of the model, a value of 1mW/m² is added to the heat flux and the model was ran again. Using a while-loop a comparison between the previous and current RMS-error can be made. The model will keep running while the new RMS-value will be lower than its predecessor but will stop once this is no longer the case. The temperature curve with the lowest RMS-error will then be exported automatically into an excel file using the Python extension *openpyxl* (Gazoni and Clark, 2016).

3.4 Adding new boreholes

3.4.1 Modelled borehole locations and history

The model will run four different boreholes on different locations across Svalbard. Firstly, DH4 will be modelled as a reference for the other models. It is located in Adventdalen and was drilled for CO₂ sequestration purposes. The borehole penetrated a reservoir that is present at a depth between 670-950m (Ogata et al., 2014b). The depth of the borehole is 972m and drilling started in 2007 (Olaussen et al., 2019).

The second borehole that was modelled is Tromsøbreen-II (7617/1-2), also referred to as the Haketangen borehole. The borehole is located in southern Spitsbergen (fig. 11) and was drilled by Polargas Prospektering KB in 1987 with the purpose of petroleum exploration (Senger et al., 2019). The depth of the borehole is 2337m.

Thirdly, a second petroleum exploration borehole called Grønfjorden-I (7714/2-1) was modelled. It is located at the foreland basin margin, adjacent to the West Spitsbergen Fold-and-Thrust Belt (fig. 11) The Grønfjorden-I borehole was the first petroleum exploration borehole on Svalbard, drilled between 1963 to 1967 by the Norsk Polar Navigasjon AS (Senger et al., 2019).

Lastly, a research borehole at the Sysselembreen moraine was modelled. The purpose of the borehole was to find a link between nearby outcrops and the subsurface. The official name of the borehole is BH 10-2008, it was drilled in 2008 and covers a depth of 1040m. Temperature logs are available for all boreholes except Grøndalen-I. Sysselembreen and DH4 have complete temperature logs, while Tromsøbreen-II has 11 temperature measurements spread over a depth between 700 and 1000m.

3.4.2. Digitizing logged boreholes

The lithological variations used for DH4 and Sysselembreen (fig. 11a, b) are generalizations of what was actually logged from the borehole cores. The remaining boreholes, Tromsøbreen-II and Grøndalen-I, don't contain generalized lithology log as presented by Henne et al. (2014). Thus, a manual digitization of these boreholes is required. The program used to digitize boreholes is WebPlotDigitizer (Rohatgi, 2017). After the borehole is digitized in WebPlotDigitizer, it can be exported as a csv-file. The csv-file can be turned into a pandas dataframe using: `pd.read_csv("file_name.csv")`. Once the dataframe has been imported into the heat flow code, the model can be started again. The geophysical parameters from DH4 are used for Tromsøbreen-II and Grøndalen-I (fig. 10a). Geophysical parameters for Sysselembreen (BH 10-2008) are measured specifically for this borehole by Henne et al. (2014) and therefore used instead of those for DH4 (fig. 10b).

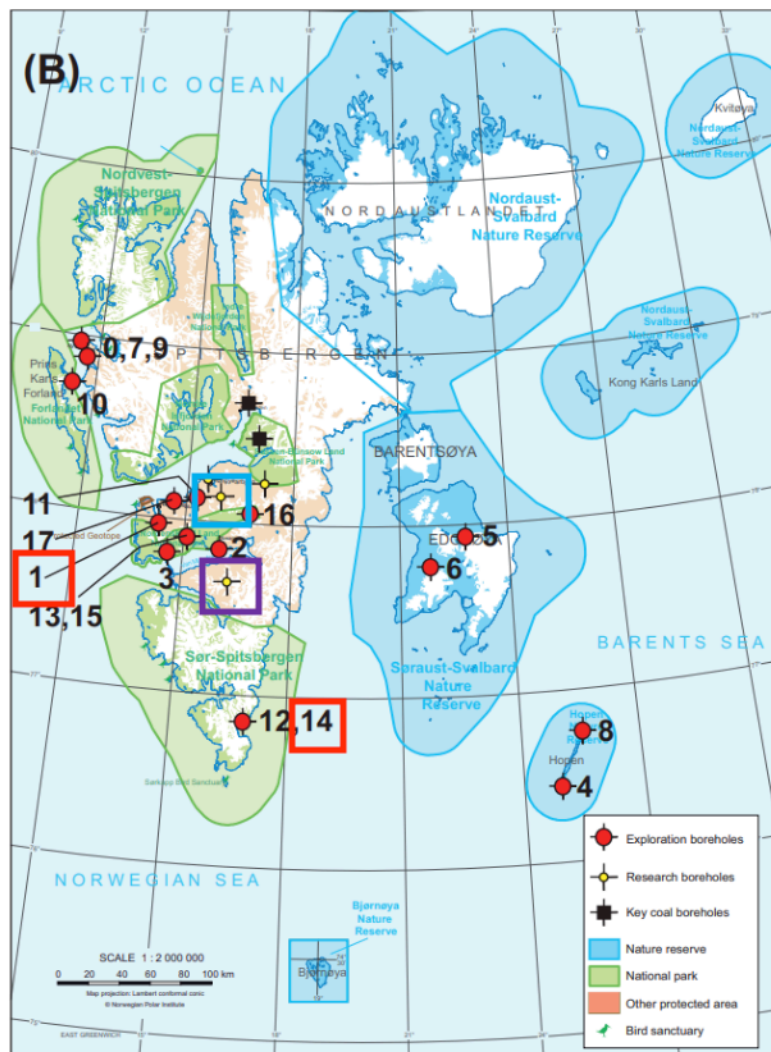


Fig.11 Location of modelled boreholes. 1, 14 (in red): Petroleum exploration boreholes; Grøndalen and Tromsøbreen-II. In blue: DH4 research borehole. In purple: Sysselembreen research borehole. (Senger et al., 2019).

4. Results

The results section is separated in two parts. The first part will present the heat flow model outcomes of the different boreholes and the second part shows the same heat flow models with adjusted parameters.

In the first part the modelled temperature graphs will be supplemented with the geothermal gradient variation over depth, RMS-error values compared to the real time temperature curve, bottom temperatures and the final- and most suitable heat flow value.

The second part will give a more detailed overview of the variation and importance of different parameters that were used as model inputs. These include material parameters (e.g. thermal conductivity, radioactive heat production), varying surface temperature and the initial model temperature.

4.1 Initial Model Results

4.1.1. Model results DH4

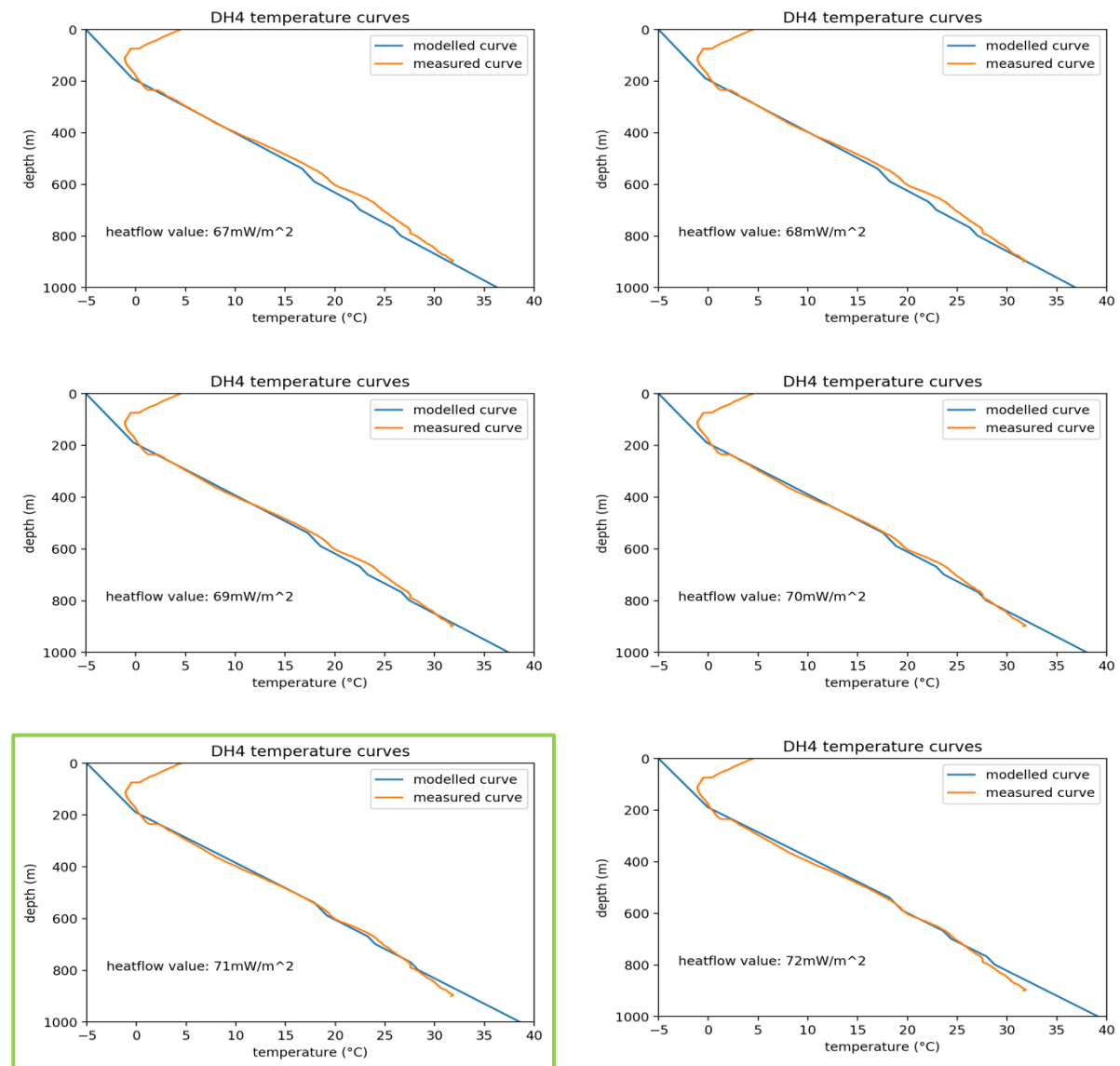


Fig. 12a-f: DH4 temperature versus depth curves with different heatflow values. Green outline indicates lowest RMS-value found.

Table 1. Value outcomes DH4 model run

Heatflow value lowest RMS	71mW/m ²
Corresponding RMS-value	2.0114
Temperature at 1000m depth	39.15 °C
Average geothermal gradient (0-1000m)*	44.14 °C/km
Average geothermal gradient (0-6000m)*	30.00 °C/km

*calculated per meter, averaged and converted from meter to kilometer scale

The lowest RMS-error value for the DH4 model run was found for a heat flow value of 71mW/m². The corresponding values such as the RMS-value and temperatures at different depths are summarized in table 1.

All modelled temperature graphs show drops and rises in the geothermal gradient on similar locations as the real temperature curve does. The graphs shift slightly upwards each time the heat flow value has risen until it the best overlap has been found. The uppermost 120m of the graphs don't seem to match, as this is still influenced by permafrost.

The bottom 100 meters of the measured temperature curve seems to have a lower geothermal gradient than what is modelled. The model with a heat flow value of 68mW/m² (fig. 12b) shows the best match when only looked at the bottom hole temperature of the measured temperatures.

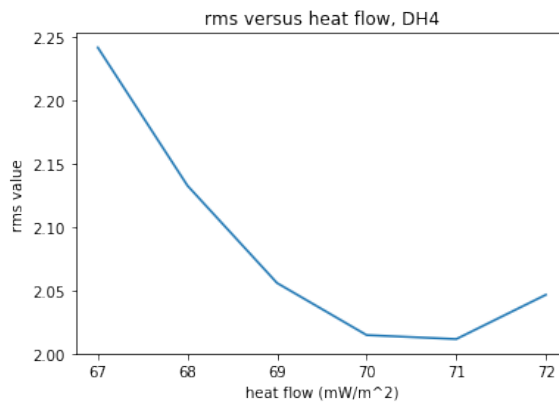


Fig. 13 RMS value versus different heat flow values, DH4

The RMS-error values plotted against their corresponding heat flow values shows a parabolic correlation. The heat flow values 70- and 71mW/m² resulted in RMS-error values with little difference, corresponding to fig. 12e and fig. 12f which also show an almost identical temperature curve.

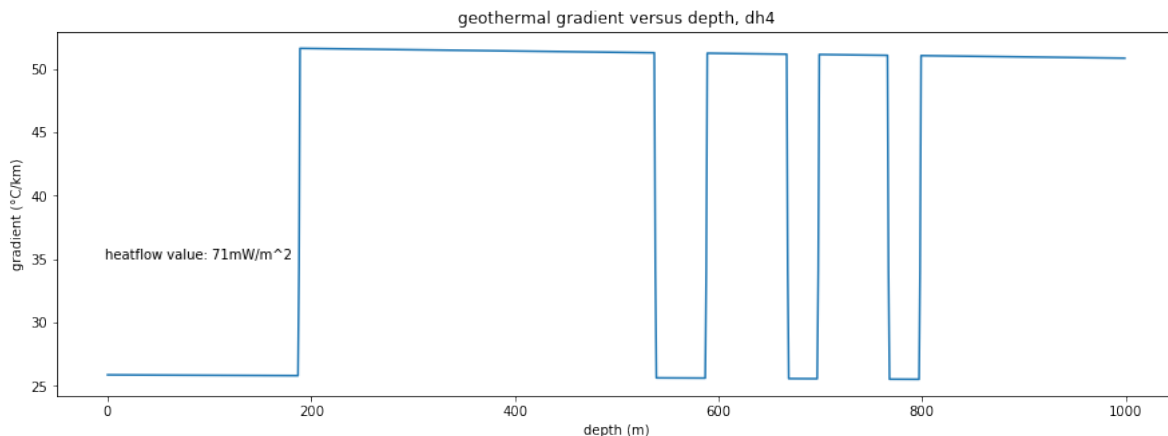


Fig. 14 Geothermal gradient per meter calculated, DH4 for 71mW/m²

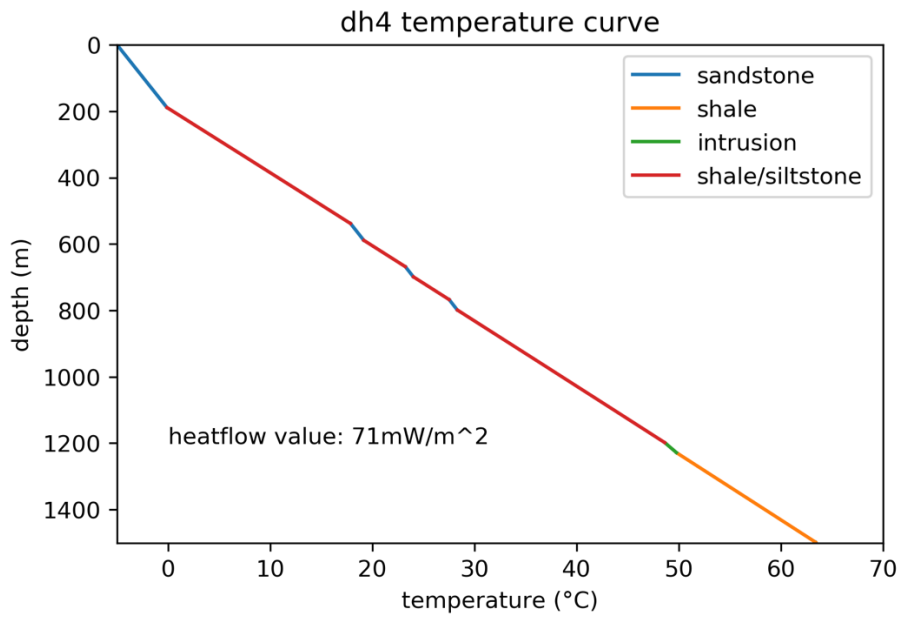


Fig. 15 Lithologies implemented in temperature curve, DH4 for 71mW/m²

The calculation of the geothermal gradient on a meter scale resulted in a step-like pattern with a general gradual decrease (fig. 14). Similar steps can be seen when the temperature graph is coloured for different lithologies (fig. 15). When the line turns from red (shale/siltstone) to blue (sandstone), the temperature increase decreases.

4.1.2 Model results Tromsøbreen-II (7617/1-2)

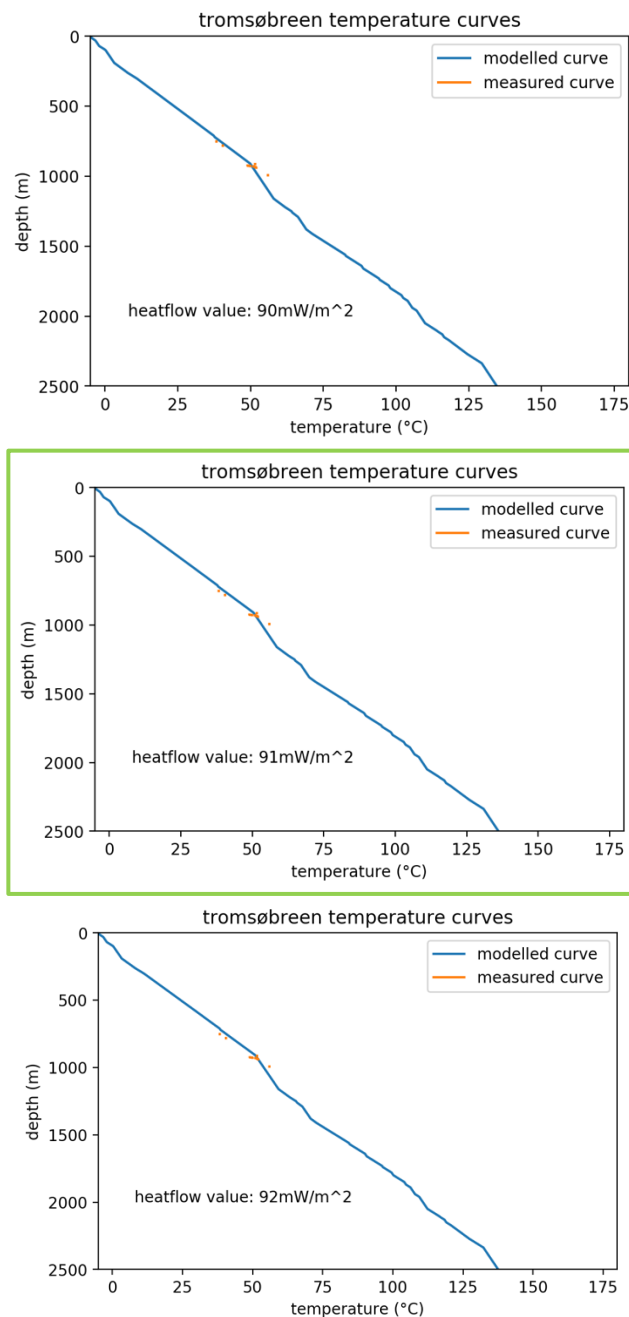


Fig. 16a-c: Tromsøbreen-II temperature versus depth curves with different heatflow values. Green outline indicates lowest RMS-value found.

The lowest heat flow value found for the lowest RMS-error value for the Tromsøbreen-II borehole was 91mW/m^2 (fig. 16b). A notable difference in temperature measurements can be seen between Tromsøbreen-II and DH4. The lack of temperature measurements for this borehole makes finding the most fitting heat flow value less reliable as less points can be compared. All temperature measurements seem to fall on the modelled curve, with the exception of the last temperature measurement.

Comparing the value outcomes of DH4 with Tromsøbreen-II (table 1, 2), a noticeable difference of over 10°C at a depth of 1000m can be seen. Average geothermal gradients of Tromsøbreen-II also exceed those of DH4

Table 2. Value outcomes Tromsøbreen-II (7617/1-2) model run

Heatflow value lowest RMS	91mW/m ²
Corresponding RMS-value	1.5648
Temperature at 1000m depth	53.84 °C
Average geothermal gradient (0-1000m)*	58.86 °C/km
Average geothermal gradient (0-6000m)*	43.14 °C/km

*calculated per meter

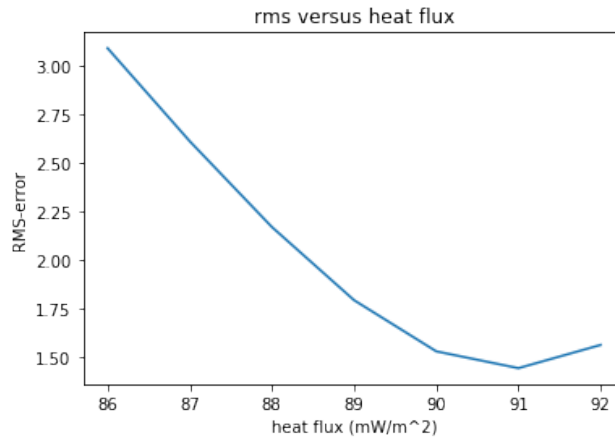


Fig. 17 RMS value versus different heat flow values, Tromsøbreen-II

The RMS-error curve for Tromsøbreen-II (fig. 17) shows a parabolic trend, similar to DH4. Generally lower RMS-values are found for Tromsøbreen-II as for DH4.

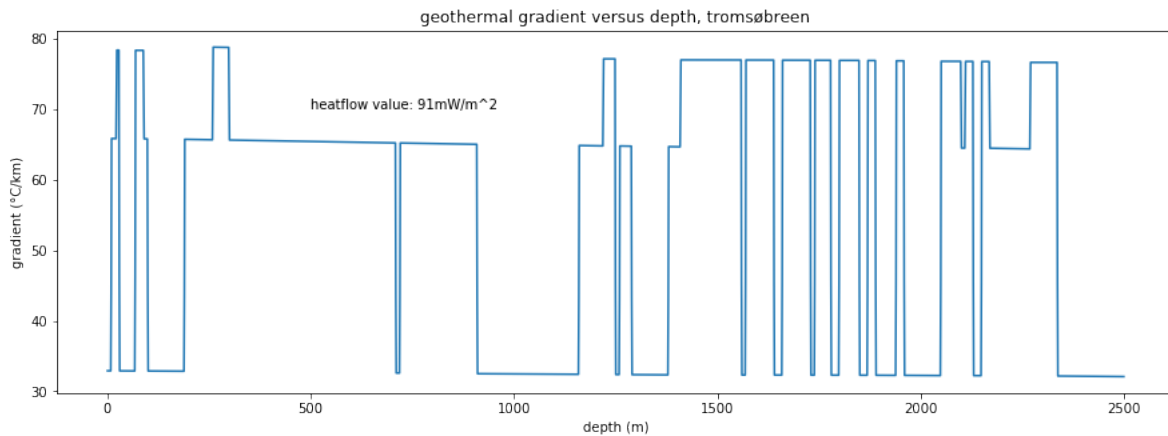


Fig. 18 Geothermal gradient per meter calculated, Tromsøbreen-II for 91mW/m²

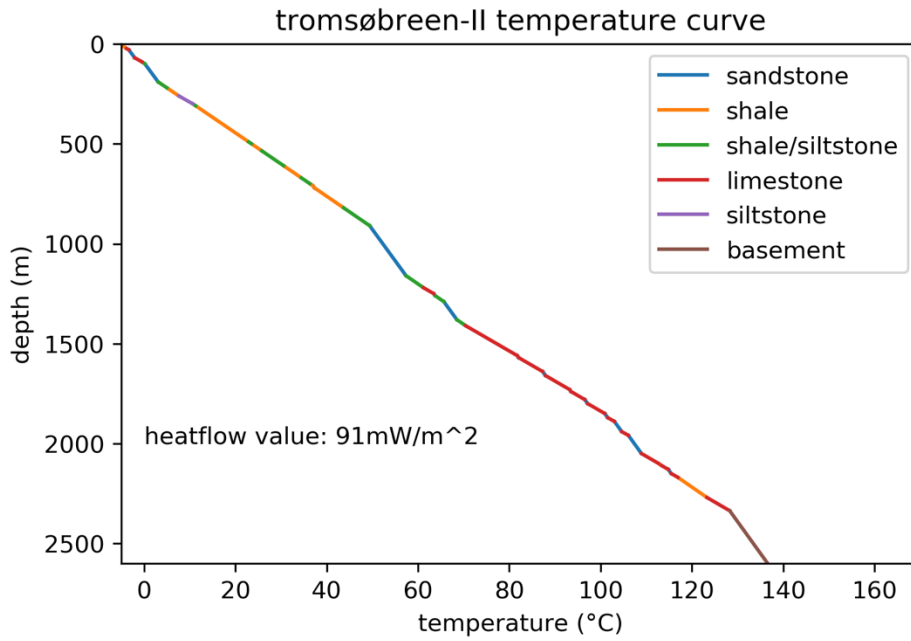


Fig. 19 Lithologies implemented in temperature curve, Tromsøbreen-II for 91mW/m²

Similar differences to the DH4 borehole in geothermal gradients between different lithologies are visible for Tromsøbreen-II. However, a geological unit that is found both in Tromsøbreen-II and DH4, does possess a higher geothermal gradient in Tromsøbreen-II. As an example, the shales at Tromsøbreen-II almost reach a value of 80°C/km whereas in DH4 a value of 51°C/km is reached (fig. 14, 18).

4.1.3 Model results Grønfjorden-I (7714/2-1)

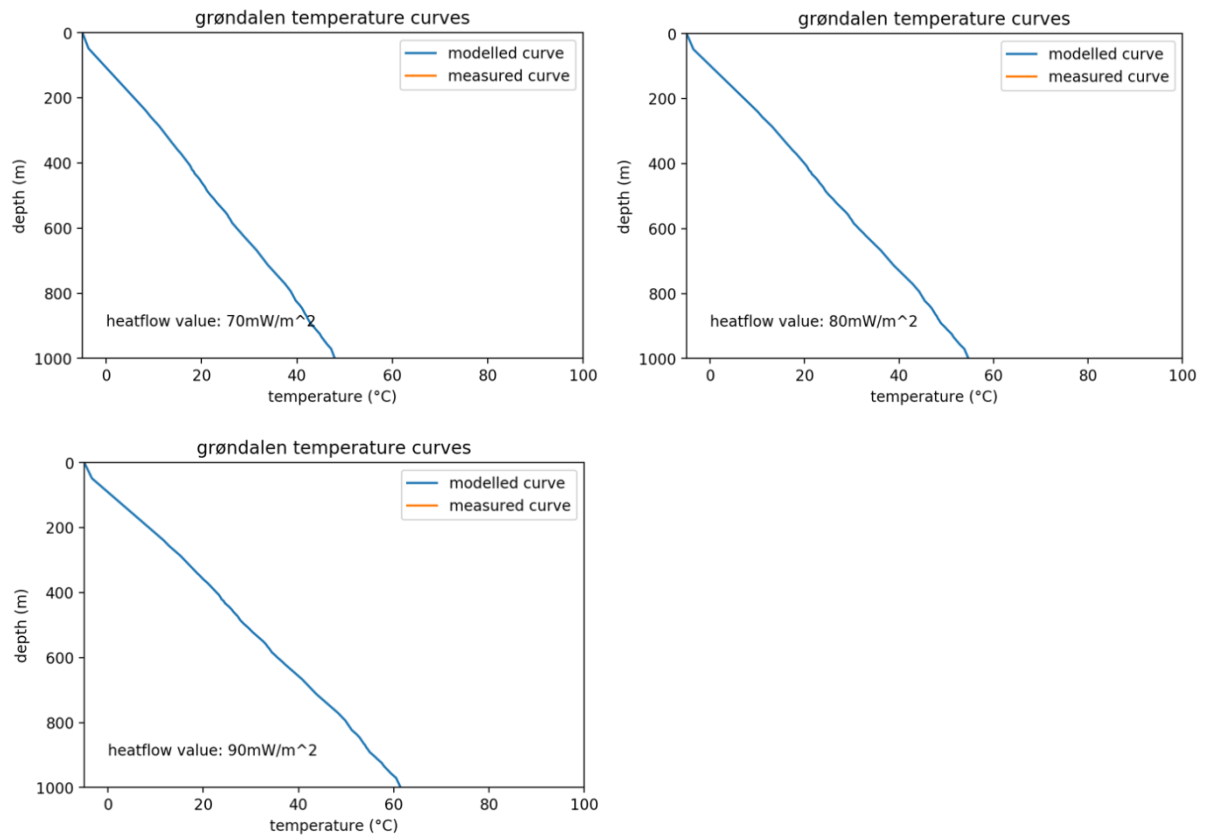


Fig. 20a-c: Grønfjorden-I temperature versus depth curves with different heatflow values. No measured temperature data available for this borehole.

Table 3. Value outcomes Grønfjorden-I (7714/2-1) model run

Temperature at 1000m depth (70mW/m ²)	47.90 °C
Average geothermal gradient (0-1000m, 70mW/m ²)	52.91 °C/km
Temperature at 1000m depth (80mW/m ²)	54.66 °C
Average geothermal gradient (0-1000m, 80mW/m ²)	59.68 °C/km
Temperature at 1000m depth (90mW/m ²)	61.43 °C
Average geothermal gradient (0-1000m, 90mW/m ²)	66.44 °C/km

The results for the Grønfjorden-I model run differ from those of DH4 and Tromsøbreen-II as no temperature data from this borehole was available. Three different heatflow values were used as an input and resulted in values shown in table 3. A remarkable difference in the average geothermal gradient value for the first 1000m is seen comparing the Grønfjorden-I model run of 70mW/m² with the 71mW/m² run for DH4, and also when comparing the 91mW/m² run for Tromsøbreen-II with the 90mW/m² run for Grønfjorden-I. Corresponding temperatures at a 1000m depth are also higher in Grønfjorden-I.

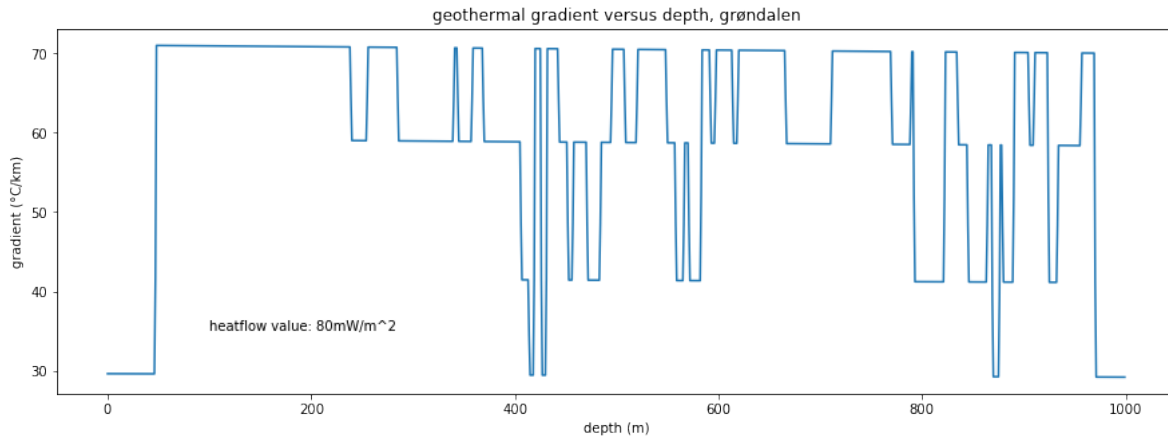


Fig. 21 Geothermal gradient per meter calculated, Grøn fjorden-I for 80mW/m²

The geothermal gradient versus depth and a lithology implemented heat flow curve were plotted against depth for a heat flow value of 80mW/m². Small intervals of a low geothermal gradient (fig. 21) are corresponding with intervals of silty sandstone and sandstone (fig. 22). In the borehole larger intervals of shale and siltstone are followed by smaller intervals sandstone (fig. 22).

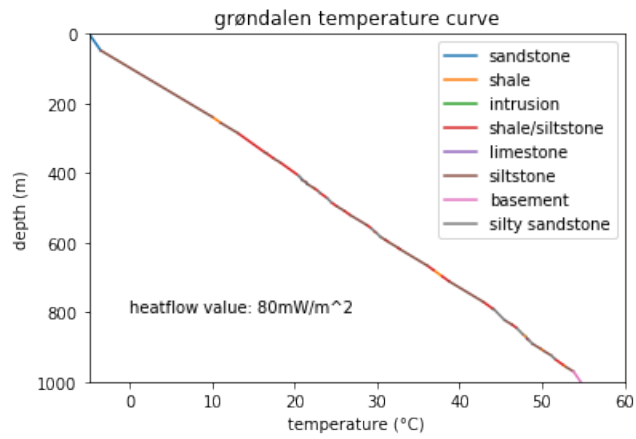


Fig. 22 Lithologies implemented in temperature curve, Grøn fjorden-I for 80mW/m²

4.1.4 Model results Sysselembreen (BH 10-2008)

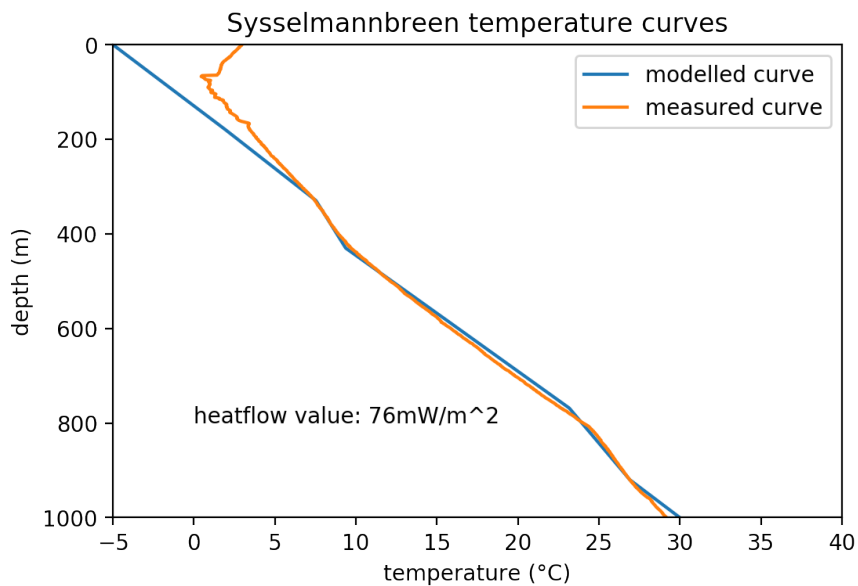


Fig. 23 Sysselembreen temperature versus depth curves

Table 4. Value outcomes Sysselembreen (BH 10-2008) model run

Heatflow value lowest RMS	76mW/m ²
Corresponding RMS-value	1.7263
Temperature at 1000m depth	29.95 °C
Average geothermal gradient (0-1000m)*	34.37 °C/km
Average geothermal gradient (0-6000m)*	27.70 °C/km

*calculated per meter

The borehole at Sysselembreen consisted of a complete temperature curve. Like DH4, this complete temperature dataset makes the RMS-error comparison of the graphs more reliable. The best match was ultimately found for a value of 76 mW/m². Despite a higher heatflow value, geothermal gradients and bottom hole temperatures are lower than DH4.

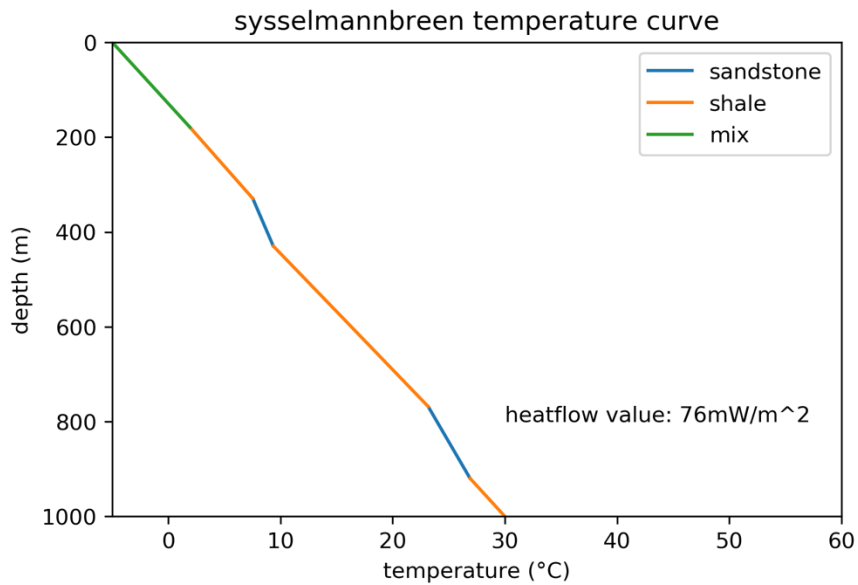


Fig. 24 Lithologies implemented in temperature curve, Sysselembreen for 76mW/m²

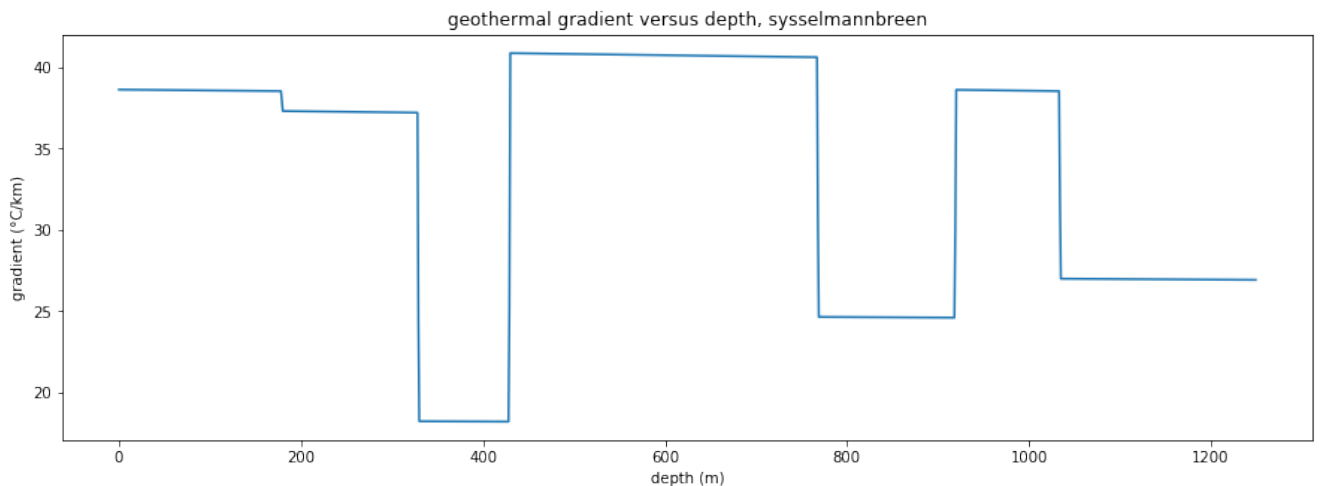


Fig. 25 Geothermal gradient per meter calculated, Sysselembreen for 76mW/m²

A difference between the geothermal gradient graphs of Sysselembreen compared to DH4 and Tromsøbreen-II can be seen as intervals of similar lithologies contain different geothermal gradients. Similar trends are still to be seen, as generally higher geothermal gradients are still found in shales and lower gradients in the sandstones.

4.2 Adjusted model parameters

To emphasize the difference parameter adjustments made to the model outcome, three extra model runs for DH4 with a heat flow value of 71mW/m^2 were made, with adjustable parameters.

The first of these model runs shows an adjustment of the thermal conductivity value for the shale unit (fig. 26). Bottom hole temperature differences of over 8°C are reached when the thermal conductivity is adjusted for.

In the second model run a comparison was made between a run with and without radioactive internal heat production (fig. 27). In the case for DH4, the differences are less than what is seen with the thermal conductivity, but bottom hole temperature differences approaching 5°C are still a remarkable change.

Lastly, the density and heat capacity values were changed. For both of these models runs no difference was seen (fig. 28 for density).

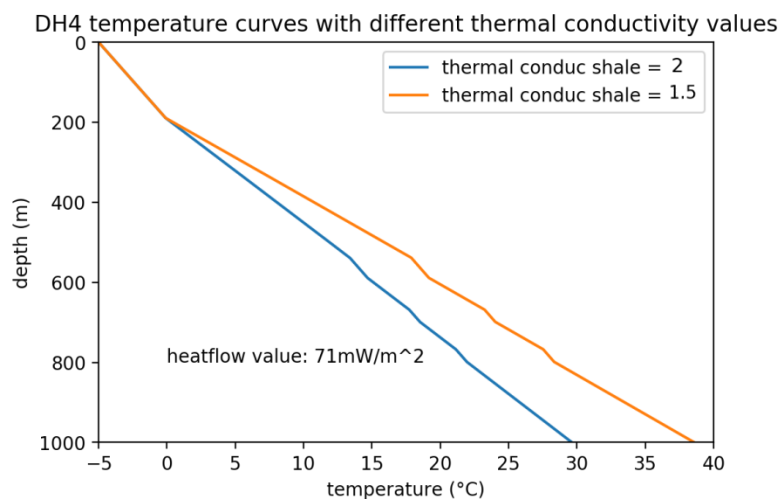


Fig. 26 Modelled temperature curves with different thermal conductivities for shale and shale/siltstone

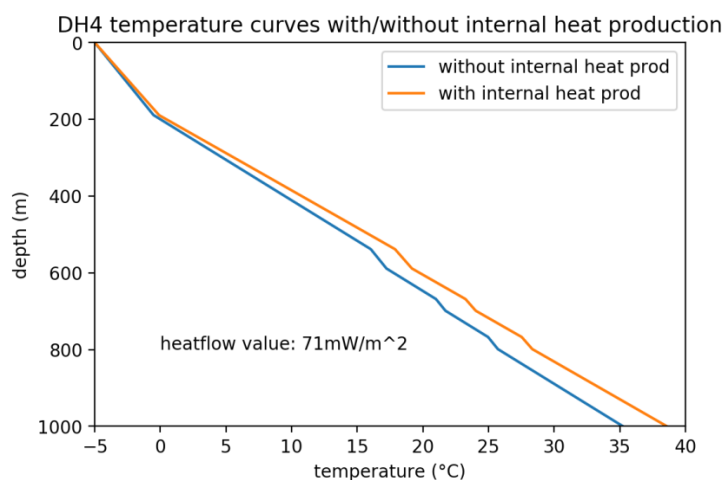


Fig. 27 Modelled temperature curves with and without radioactive internal heat production

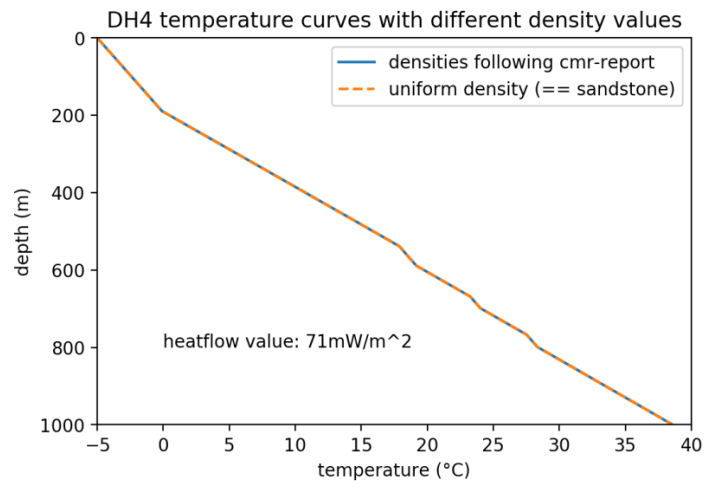


Fig. 28 Modelled temperature curves with uniform and actual densities

5. Discussion

5.1 Model outcomes and constraints

5.1.1 DH4

The purpose of the DH4 model run was to serve as a reference run to see whether or not the model produced results that fell in the desired error range. The Adventdalen area, surrounding the DH4 area, has heat flow values between 60-90 mW/m² (Pascal et al., 2010), a study by Tsibulya and Sokolova (2002) also suggests values between 70-80 mW/m² for the Nordenskiöldland area (fig. 29). Furthermore, a COMSOL model by Henne et al. (2014) resulted in a final heatflow value of 70mW/m² for DH4 specifically. In order to calibrate the model, the lowest found RMS-error value had to coincide with the range specified by Beka et al. (2015) and approach the value modelled by Henne et al. (2014).

The first working model run included surface temperature variations, material parameters as shown in fig. 11, but excluded internal heat production. The outcome of this model run was above 90mW/m² and had to be corrected for. After implementing radioactive heat production as an explicit SourceTerm in the heat flow equation (eq. 2.5) the heat flow value for the lowest RMS-error value dropped to 91mW/m².

A correction to the thermal conductivity in the shale and shale/siltstone from 2.0 to 1.5 W/mK was made to drop the value down to 71mW/m². A similar adjustment was made by Henne et al. (2014). As seen in fig. 12e, the model now overlaps sufficiently with the exception of the uppermost 200 meters that is affected by permafrost. This can be ignored as this part of the temperature curve is highly dependent on the time of the year when the temperature is measured.

The choice to lower the thermal conductivity value for shale and shale/siltstone in the model created by Henne et al. (2014) isn't supported by experimental data. In order to say with more certainty that the outcome of the current models is correct, a new set of experiments regarding the thermal conductivity of shale and silty shale have to be conducted. If it is the case that the thermal conductivity is 2.0 W/mK, the heat flow values for DH4 are much higher than expected by previous work (Henne et al., 2014, Beka et al., 2015, Tsibulya and Sokolova, 2002).

For the two other boreholes the value for shale and silty shale are kept on 1.5 W/mK as heat flow values would otherwise reach values far above values found by previously done work. The need for good data regarding thermal conductivity is hereby emphasized. Fig.23 also shows how different temperature curves for DH4 would look for different thermal conductivity values with a similar heat flow value. Density and heat capacity have not shown an effect on the final temperature curve (fig. 28) but do affect the convergence time of the model.

The graph showing the geothermal gradient evolution over depth (fig. 14) was made to illustrate the importance of the geology in the temperature curve as geothermal gradient drops of over 20°C/km are seen when the geology changes from shale to sandstone. This graph coincides with the geothermal gradient column by Railsback (2011) in fig.7. The temperature curve with implemented lithologies (fig. 15) confirms this as bends in the temperature curve can be seen where a lithology change occurs.

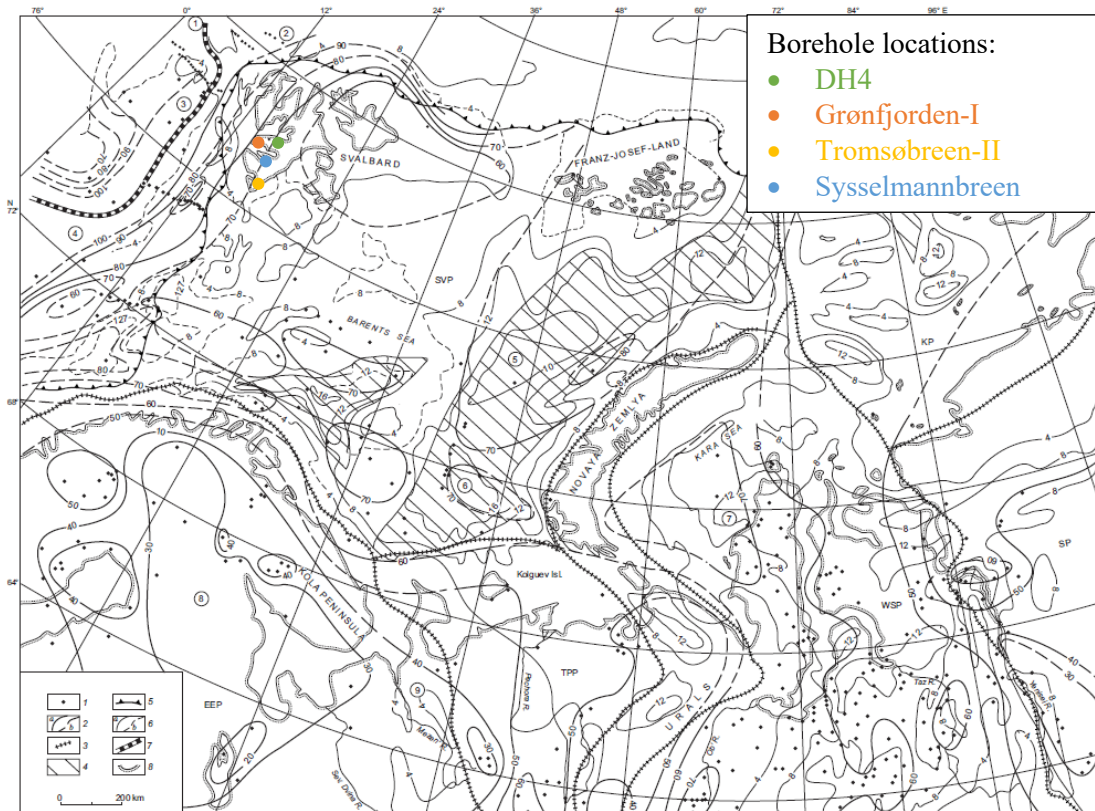


Fig. 29 Heat flow map of Barentz and Kara seas. Dots approximating the borehole locations. (Tsubilya and Sokolova, 2002)

5.1.2 Tromsøbreen-II (7617/1-2)

The measured borehole temperatures at Tromsøbreen-II exceed those of DH4 by more than 10°C at a depth of 1000m (table 1, table 2). Using the same parameters as for DH4, a heat flow value of 91mW/m² was found. Choosing the same parameters comes at a cost of another uncertainty, as geophysical parameters can differ laterally. In the case for the Tromsøbreen-II dataset, the uppermost 1400m comprises Cretaceous to Early Triassic strata. The DH4 dataset is of the same geological age which could be an argument supporting the use of the same parameters. The Tromsøbreen-II borehole reaches a larger depth and continues down to the late Carboniferous. These older strata may be of similar lithology but can possess substantially different geophysical properties. An example for this uncertainty can be seen when comparing the geophysical properties of a borehole at Sysselembreen (fig. 11b) with those used for DH4 and thus Tromsøbreen-II. The shales and sandstones from the Eocene and Paleocene found at Sysselembreen differ mostly in their thermal conductivity. As described in section 4.2, this parameter has shown to be of importance to the model outcomes and therefore adds to the uncertainty of the modelling for lower strata at Tromsøbreen-II.

Temperature measurements from this borehole are scarce, only comprising of around 10 measurement of which all are at a depth between 750 and 1000m. The scarcity of the temperature dataset affects the precision of the model outcome as less points can be compared with one another.

However, the model proves to be of good use in a scenario as encountered for Tromsøbreen-II. On a place where little temperature data is available, the model can be used to supplement with modelled temperature data. Despite the few datapoints, the RMS-error can still be calculated, and the best fitting curve can then give an indication of the temperature curve that could have been measured.

5.1.3 Grønfjorden-I (7714/2-1)

No temperature data was available for Grønfjorden-I and therefore a lowest RMS-error value could not be found. In a situation as such, the model can still become useful when heatflow values are roughly known and one is interested to know about the temperature curve. However, heatflow values around Svalbard fall in a range of 60-90mW/m² (Beka et al., 2015) which makes the range rather large. The three model outputs for Grønfjorden-I (fig. 20a-c) show what the temperature curves could look like for three different heatflow values. As is shown in table 3, a heatflow value difference of 10mW/m² impacts temperatures at 1000m depth by more than 5°C. As seen in fig.22, the borehole comprises mostly of shale and siltstone which both have a low thermal conductivity (fig. 7, 11). This has resulted higher bottom hole temperatures for Grønfjorden-I compared to both DH4 and Tromsøbreen-II with similar heat flow value inputs. For a heat flow value of 70mW/m², the temperature at Grønfjorden-I exceeds the bottom hole temperature at DH4, for a heat flow value of 71mW/m², by 9°C. Similarly, the bottom hole temperature at Tromsøbreen-II for similar heat flow values (90mW/m² vs. 91mW/m²) is exceeded by almost 13°C.

5.1.4 Sysselmannbreen (BH 10-2008)

The borehole at Sysselmannbreen is in its completeness of data similar to DH4, but penetrates younger sedimentary strata. For every meter there is a temperature measurement making a heat flow value based on RMS-error values more certain.

Bottom hole temperatures at this borehole are in comparison to other boreholes low, despite having a higher heat flow value input. This can be explained by the higher values for thermal conductivity for both the shales and sandstones (fig. 11) (Henne et al., 2014). As described in section 5.1.1, a much higher value for the heat flow value was found for DH4 when the old thermal conductivity value of 2.0mW/k was still used (Henne et al., 2014).

The final heat flow value that resulted from this model run (table 4.) is higher than previously suggested value of 70mW/m² by Henne et al. (2014) (fig. 9) and lower than the 80mW/m² as suggested by Pascal et al. (2010). The difference with the work done by Pascal et al. (2010) is mostly due to the usage of a different heat flow estimation technique, which in this case is the "Bullard Method", which is an estimation technique using a Bullard plot in which the thermal resistance is plotted against the temperature. The heat flow is then indicated by the steepness of the curve.

5.3 Geological link to geothermal trends

The heat flow values ranging from 60mW/m^2 to 90mW/m^2 across Spitsbergen are considered to be reasonably large ($>50\text{mW/m}^2$), compared to mainland Norway (Beka et al., 2015) (Khutorskoi et al., 2009). Up to 60% of the surface heat flow is attributed to mantle heat flow under continents (Pollack and Chapman, 1977), indicating a thinned lithosphere for Svalbard (Beka et al., 2015). The thinned lithosphere is thought to be associated with an uplift event during the Cenozoic (Vågnes and Amundsen, 1993). The estimated uplift values (fig. 30) show that the highest uplift values fall within the Central Tertiary Basin. This explains the higher values of around 70mW/m^2 found across the basin but doesn't yet explain the anomalies at Tromsøbreen-II and Bockfjorden (fig. 31).

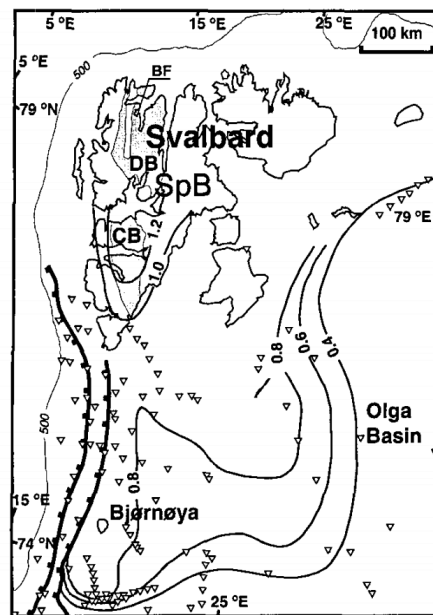
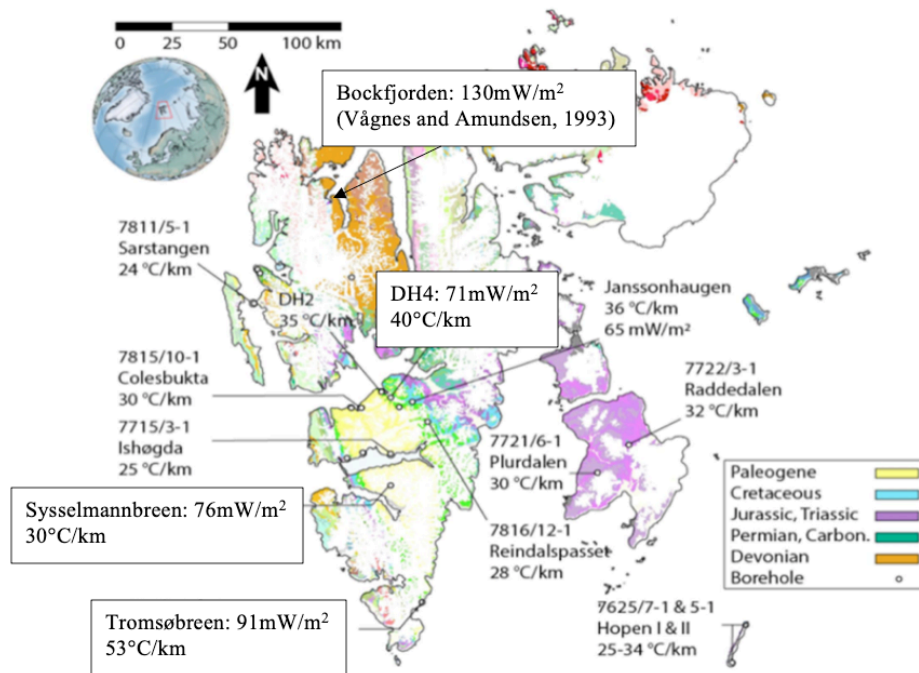


Fig. 30 Estimated tectonic uplift relative to present sea level. (Vågnes and Amundsen, 1993)

These values exceed those expected to be caused by the uplift event and another factor has to attribute to this anomaly in order to explain it. In the case for the anomaly at Bockfjorden, it is most likely linked to a convective heat transfer as the area is known for emerging hot springs (Vågnes and Amundsen, 1993). The hot springs at Bockfjorden formed along a N-S trending fault (fig. 5,6) which hosts fluid pathways in surrounding fracture networks. Numerous other hot springs in western Svalbard can be found along N-S trending fault zones laying parallel to the Cenozoic Hornsund-De Geer Fault Zone transform plate boundary (fig. 5) (Dallmann, 1999). Boreholes that are being drilled in close proximity may be affected by convective heat transfer related to these hot springs.

Both Tromsøbreen-II and Bockfjorden have shown heat flow anomalies due to their proximity to a hot spring. In the case for Bockfjorden, the heat flow anomaly and the occurrence of the hot spring can be related to a presence of a nearby volcanic complex (Vågnes and Amundsen, 1993) Another N-S trending fault zone, hosting two hot springs, can be found in the vicinity of Grønfjorden-I borehole. Whether or not this borehole is affected by the fault zone cannot be told without temperature measurements, but its proximity to the hot springs might indicate a higher heat flow than those found more central in the Central Tertiary Basin.



*Fig. 31 Modified heat flow and geothermal gradient map of Svalbard.
From (Betlem et al., 2018)*

All previously known geothermal gradients and heat flow measurements of boreholes were summarized in fig.8. The newly modelled results together with a heat flow measurement of a hot spring (Vågnes and Amundsen, 1993) were added to create a newly updated overview map (fig. 31). The geothermal trend that can be seen in fig.31 can be related to a Cenozoic uplift event and convective heat transfer along fault zones. Higher heat flow values can be found more central in the basin as the uplift is highest (fig. 30).

5.4 Geothermal energy on Svalbard and future work

The temperature profiles that were created using the heat flow model in section 4, combined with the Lindal diagram (fig. 4) can provide useful information regarding potential geothermal applications for Svalbard.

At a depth of 1000m, a temperature of 39°C would be insufficient to generate electricity using the geothermal energy system as shown in fig.3. According to the Lindal diagram (fig. 4), temperatures in this range can be used for heating systems. Temperatures suitable for energy generating systems are found below 2500m depth, within the Devonian strata. Whether or not it is possible and economical to drill this deep, has to be further investigated. The Devonian strata also needs to fulfill the requirements for a geothermal energy system. Permeability, pressure and presence of a cap rock are factors that will have to be further looked into.

The borehole at Tromsøbreen-II reached much higher temperatures at shallower depths compared to DH4 and even surpasses required temperature values necessary to generate electricity. Whether or not a possible geothermal reservoir is present could be investigated using resistivity measurements. The main issue with this borehole is its remoteness from the Svalbard settlements and strict environmental restrictions being located within a national park.

A temperature gradient of 0.079°C/m (or 79°C/km) is found for the Bockfjorden area as suggested by xenolithic evidence from Quaternary volcanism (Amundsen et al., 1988). The area has undergone crustal uplift, mantle lithosphere thinning and Neogene volcanism (Vågnes and Amundsen, 1993). This had led to a local heat flow value of 130mW/m² combined with a geothermal gradient of 79°C/km and the presence of hot springs with temperatures up to 25.6°C (Banks et al., 1998). The area makes an interesting study for further geothermal energy research as the values found here approach those found e.g. in northern Iceland (Friðleifsson, 1994). Whether or not the Devonian basin is suitable for hosting a geothermal reservoir will have to be further looked into. The remoteness of the area could make the energy extraction not worthwhile.

Heat flow values at Sysselembreen were rather high and would suggest potential geothermal applications. However, a large amount of high conducting layers negatively impacts the temperature curve and therefore a relatively low geothermal gradient was measured and calculated for this area. With a geothermal gradient of below 30°C/km one has to drill rather deep in order to exploit this area. Like Tromsøbreen-II, the location of this borehole is remote, and geothermal exploitation would most likely be uneconomical.

Lastly, the borehole at Grønfjorden-I didn't contain any temperature measurements and therefore an assessment of a potential geothermal application can't be made with any certainty. If according to the hypothesis stated in section 5.3, a high heat flow value would be found for this borehole due to convective heat from the fault networks, it might be a potential candidate. As seen in section 4.1.4, temperatures reached in this borehole were relatively large compared to the heat flow values. The boreholes proximity to the mining town Barentsburg could potentially mean it is economic enough for exploitation.

In order to assess geothermal applications with more ease, models as those made in this thesis could be expanded into 2D and 3D models. Combined with more knowledge regarding reservoirs, the geothermal energy exploitation can be improved.

6. Conclusions

This thesis provided FiPy-based temperature models that aided a geothermal energy assessment for Svalbard. This was made possible by combining knowledge in physics, geology and modelling. In the theoretical background in which these key fields were explained, the reader was introduced or familiarized with the heat flow equation, the base of the model to be constructed. How the heat flow equation was to be implemented within Python was then addressed in the modelling section. By providing geological background information to a temperature profile producing heat flow model, trends and relations between heat flow, geothermal gradients and regional geology were made.

The heat flow model resulted in three heat flow values for the boreholes DH4, Tromsøbreen-II (7617/1-2) and Sysselembreen (BH 10-2008). These were respectively 71mW/m², 91mW/m² and 76mW/m². As Grønfjorden-I (7714/2-1) didn't contain a temperature profile, a heat flow value couldn't be found. By inputting assumed heat flow values for Grøndalen-I, assumed temperature profiles of this borehole were made.

The results were being put in perspective by looking at the influence of individual model parameters. Changes of the thermal conductivity and internal radiogenic heat production were shown to make a difference in the temperature profile. This led to a discovery of uncertainty in the model. The parameters found for DH4, used for Tromsøbreen-II and Grønfjorden-I, differed from those found for Sysselembreen, ultimately resulting in a lower geothermal gradient for Sysselembreen despite a higher heat flow value and abundance of shale (the lithology with the lowest thermal conductivity found). To lower the uncertainty of the model outcomes for Grøndalen-I and Tromsøbreen-II, borehole samples will have to be measured for geophysical parameters.

High heat flow values for Svalbard (>70mW/m²) can be related to a crustal uplift episode during the Cenozoic. The uplift is thought to be the highest within the Central Tertiary Basin, in which values above 70mW/m² were indeed found for DH4 and Sysselembreen. The heat flow value found for Tromsøbreen-II couldn't be explained for using only the uplift episode and is thought to exceed the values of the other boreholes due to its proximity to a N-S trending fault network hosting hot fluid pathway. A heat flow value of 130mW/m² was found for an area close to a similar fault network hosting thermal springs, linked to Neogene volcanic events.

Based on the Lindal Diagram, potential geothermal applications were discussed for the boreholes. Temperatures found for DH4 were too low to produce electricity, however other applications can be considered, such as space heating. The area contains a reservoir which could potentially be used as a geothermal reservoir. The higher geothermal gradients found for the Bockfjorden area and at Tromsøbreen-II reach high enough temperatures within a reasonable depth to be considered for electricity production. However, the presence of a reservoir in these areas is unknown, and their remoteness could make exploitation uneconomical. Further research regarding Grønfjorden-I is highlighted as its proximate to a N-S fault network, which could host hot fluid pathways influencing the heat flow. The borehole contains large intervals of low thermal conductivity units that increase the geothermal gradient. Grønfjorden-I is nearby the Russian mining town Barentsburg, which

could make geothermal exploitation more economical compared to the Bockfjorden and Tromsøbreen areas

As the Arctic region continues to warm, need for more knowledge regarding renewable energy sources is of high importance. By creating a model that provides a framework for finding temperature curves or heat flow values across Svalbard, a contribution to this knowledge was made. The model for now is only applicable for 1D borehole scenarios, but when expanded into a second or third dimension, could be a good step towards a much more advanced geothermal energy assessments for Svalbard.

7. References

- Amundsen, H., Griffin, W., and O'REILLY, S., 1988, The nature of the lithosphere beneath northwestern Spitsbergen: xenolith evidence.
- Anderson, T. R., Hawkins, E., and Jones, P. D., 2016, CO₂, the greenhouse effect and global warming: from the pioneering work of Arrhenius and Callendar to today's Earth System Models: *Endeavour*, v. 40, no. 3, p. 178-187.
- Banks, D., Sletten, R. S., Haldorsen, S., Dale, B., Heim, M., and Swensen, B., 1998, The thermal springs of Bockfjord, Svalbard: occurrence and major ion hydrochemistry: *Geothermics*, v. 27, no. 4, p. 445-467.
- Barbier, E., 2002, Geothermal energy technology and current status: an overview: *Renewable and sustainable energy reviews*, v. 6, no. 1-2, p. 3-65.
- Beka, T. I., Smirnov, M., Bergh, S. G., and Birkelund, Y., 2015, The first magnetotelluric image of the lithospheric-scale geological architecture in central Svalbard, Arctic Norway: *Polar Research*, v. 34, no. 1, p. 26766.
- Betlem, P., 2018, Geothermal Gradients on Svalbard, Arctic Norway.
- Braathen, A., Bælum, K., Christiansen, H. H., Dahl, T., Eiken, O., Elvebakk, H., Hansen, F., Hanssen, T. H., Jochmann, M., and Johansen, T. A., 2012, The Longyearbyen CO₂ Lab of Svalbard, Norway—initial assessment of the geological conditions for CO₂ sequestration: *Norwegian Journal of Geology/Norsk Geologisk Forening*, v. 92, no. 4.
- Buonsanti, F., 2011, Promoting Renewable Energy in Longyearbyen: A Sustainable Means to Prevent Svalbard's Environmental Degradation: *Consilience*, no. 6, p. 192-209.
- Dallmann, W., 1999, Lithostratigraphic lexicon of Svalbard, Norwegian Polar Institute.
- Dallmann, W. K., Elvevold, S., Gerland, S., Hormes, A., Majka, J., Ottemöller, L., Pavlova, O., and Sander, G., 2015, Geoscience Atlas of Svalbard, Norsk polarinstitutt.
- Friðleifsson, G. Ó., 1994, Geothermal gradient and hydrothermal systems off North Iceland, Statement GÓF-94-05, Reykjavik, Orkustofnun, National Energy Authority Iceland, p. 4.
- Gazoni, E., and Clark, C., 2016, openpyxl-A Python library to read/write Excel 2010 xlsx/xlsm files: Retrieved from.(accessed on 20 April 2016) <http://openpyxl.readthedocs.org/en/default>.
- Gerlach, J., and Kinossian, N., 2016, Cultural landscape of the Arctic: 'recycling' of soviet imagery in the Russian settlement of Barentsburg, Svalbard (Norway): *Polar Geography*, v. 39, no. 1, p. 1-19.
- Guyer, J. E., Wheeler, D., and Warren, J. A., 2009, FiPy: Partial differential equations with Python: *Computing in Science & Engineering*, v. 11, no. 3, p. 6-15.
- Hagen, D., Erikstad, L., Flyen, A. C., Hanssen, S. A., Moe, B., Olsen, S. L., and Veiberg, V., 2018, Avslutningsplan for Svea. Kunnskapsstatus for naturmiljø og kulturmiljø.
- Henne, I., Kocbach, J., and Hauge, R., 2014, Thermal modelling of the subsurface in Adventdalen and Sysselmannbreen at Svalbard using COMSOL Multiphysics.
- Hirschberg, S., Wiemer, S., and Burgherr, P., 2014, Energy from the Earth: Deep Geothermal as a Resource for the Future?, vdf Hochschulverlag AG.
- Huenges, E., and Ledru, P., 2011, Geothermal energy systems: exploration, development, and utilization, John Wiley & Sons.
- Hurley, B. W., 2009, Natural radioactivity in the geologic environment.
- Iversen, J., 2013, Geothermal energy and district heating in Ny-Ålesund, Svalbard: UiT The Arctic University of Norway.
- Jones, M., 1992, Heat flow anomaly in Lesotho: implications for the southern boundary of the Kaapvaal craton: *Geophysical Research Letters*, v. 19, no. 20, p. 2031-2034.

- Khutorskoi, M., Leonov, Y. G., Ermakov, A., and Akhmedzyanov, V., Abnormal heat flow and the trough's nature in the Northern Svalbard plate, *in* Proceedings Doklady Earth Sciences 2009, Volume 424, Springer Science & Business Media, p. 29.
- Kristmannsdóttir, H., and Ármannsson, H., 2003, Environmental aspects of geothermal energy utilization: Geothermics, v. 32, no. 4-6, p. 451-461.
- Krzyszowska, A. J., 1985, Tundra degradation in the vicinity of the Polish Polar Station, Hornsund, Svalbard: Polar Research, v. 3, no. 2, p. 247-252.
- Labus, M., and Labus, K., Thermal conductivity of fine-grained sedimentary rocks, *in* Proceedings Central and Eastern European Conference 2017, p. 323-323.
- Lindal, B., 1973, Industrial and other applications of geothermal energy: Geothermal energy, p. 135-148.
- Lüning, S., and Kolonic, S., 2003, Uranium spectral gamma-ray response as a proxy for organic richness in black shales: Applicability and limitations: Journal of petroleum geology, v. 26, no. 2, p. 153-174.
- Ma, Y., Somayazulu, M., Shen, G., Mao, H.-k., Shu, J., and Hemley, R. J., 2004, In situ X-ray diffraction studies of iron to Earth-core conditions: Physics of the Earth and Planetary Interiors, v. 143, p. 455-467.
- McKinney, W., 2011, pandas: a foundational Python library for data analysis and statistics: Python for High Performance and Scientific Computing, v. 14, no. 9.
- Midttømme, K., Henne, I., Kocbach, J., and Ramstad, R. K., Geothermal Energy Use, Country Update for Norway, *in* Proceedings European Geothermal Congress 2013 2013.
- Ogata, K., Senger, K., Braathen, A., Tveranger, J., and Olaussen, S., 2014a, Fracture systems and mesoscale structural patterns in the siliciclastic Mesozoic reservoir-caprock succession of the Longyearbyen CO₂ Lab project: Implications for geological CO₂ sequestration in Central Spitsbergen, Svalbard: Norwegian Journal of Geology/Norsk Geologisk Forening, v. 94.
- Ogata, K., Senger, K., Braathen, A., Tveranger, J., and Olaussen, S., 2014b, The importance of natural fractures in a tight reservoir for potential CO₂ storage: a case study of the upper Triassic–middle Jurassic Kapp Toscana Group (Spitsbergen, Arctic Norway): Geological Society, London, Special Publications, v. 374, no. 1, p. 395-415.
- Ohm, S. E., Larsen, L., Olaussen, S., Senger, K., Birchall, T., Demchuk, T., Hodson, A., Johansen, I., Titlestad, G. O., and Karlsen, D. A., 2019, Discovery of shale gas in organic rich Jurassic successions, Adventdalen, Central Spitsbergen, Norway.
- Olaussen, S., Senger, K., Braathen, A., Grundvåg, S.-A., and Mørk, A., 2019, You learn as long as you drill; research synthesis from the Longyearbyen CO₂ Laboratory, Svalbard, Norway.
- Olsen, J., Hovelsrud, G. K., and Kaltenborn, B. P., 2020, Increasing shipping in the Arctic and local communities' engagement: A case from Longyearbyen on Svalbard, Arctic Marine Sustainability, Springer, p. 305-331.
- Omer, A. M., 2008, Ground-source heat pumps systems and applications: Renewable and sustainable energy reviews, v. 12, no. 2, p. 344-371.
- Pascal, C., Balling, N., Barrere, C., Davidsen, B., Ebbing, J., Elvebakk, H., Mesli, M., Roberts, D., Slagstad, T., and Willemoes-Wissing, B., 2010, HeatBar final report 2010. Basement heat generation and heat flow in the western Barents Sea* importance for hydrocarbon systems: NGU Report, v. 30.
- Polarinstitutt, N., 2015, Svalbardkartet: Norsk Polarinstitutt WebGIS.
- Pollack, H. N., and Chapman, D. S., 1977, Mantle heat flow: Earth and Planetary Science Letters, v. 34, no. 2, p. 174-184.

- Rachlewicz, G., Szczuciński, W., and Ewertowski, M., 2007, Post-“Little Ice Age” retreat rates of glaciers around Billefjorden in central Spitsbergen, Svalbard: *Polish Polar Research*, v. 28, no. 3, p. 159-186.
- Railsback, L., 2011, Petroleum Geoscience and Subsurface Geology: UGA Sedimentary Geochemistry Laboratory, Department of Geology, University of Georgia <http://www.gly.uga.edu/railsback/PGSG/FlatSpotsBrightSpots01.pdf>.
- Rohatgi, A., 2017, WebPlotDigitizer, Austin, Texas, USA.
- Russell, W., 1942, Radioactivity of Sedimentary Rocks.
- Sanner, B., Andersson, O., Eugster, W., and Arrizabalaga, I., 2011, Geotrained training manual for drillers of shallow geothermal systems: Brussels: GEOTRAINET. Dostopno na: <http://geotrained.eu/wpcontent/uploads/2015/11/Drillers-Manual-Final-V2-10.11.pdf>, v. 27, no. 3, p. 2019.
- Schön, J. H., 2015, Physical properties of rocks: Fundamentals and principles of petrophysics, Elsevier.
- Sclater, J., Jaupart, C., and Galson, D., 1980, The heat flow through oceanic and continental crust and the heat loss of the Earth: *Reviews of Geophysics*, v. 18, no. 1, p. 269-311.
- Senger, K., Brugmans, P., Grundvåg, S.-A., Jochmann, M. M., Nøttvedt, A., Olaussen, S., Skotte, A., and Smyrak-Sikora, A., 2019, Petroleum, coal and research drilling onshore Svalbard: a historical perspective.
- Senger, K., Tveranger, J., Braathen, A., Olaussen, S., Ogata, K., and Larsen, L., 2015, CO₂ storage resource estimates in unconventional reservoirs: insights from a pilot-sized storage site in Svalbard, Arctic Norway: *Environmental Earth Sciences*, v. 73, no. 8, p. 3987-4009.
- Shears, J., Theisen, F., Bjørdal, A., and Norris, S., 1998, Environmental impact assessment: Ny-Ålesund international scientific research and monitoring station, Svalbard.
- Skjelkvåle, B.-L., Amundsen, H., O'Reilly, S. Y., Griffin, W., and Gjelsvik, T., 1989, A primitive alkali basaltic stratovolcano and associated eruptive centres, northwestern Spitsbergen: volcanology and tectonic significance: *Journal of Volcanology and Geothermal Research*, v. 37, no. 1, p. 1-19.
- Sund, M., 2008, Polar hydrology. Norwegian Water Resources and Energy Directorate's work in Svalbard. NVE Report 2: Water Resources and Energy Directorate, Oslo.
- Svendsen, J. I., and Mangerud, J., 1997, Holocene glacial and climatic variations on Spitsbergen, Svalbard: *The Holocene*, v. 7, no. 1, p. 45-57.
- Tsibulya, L., and Sokolova, L., 2002, Heat flow in the region of the Barents and Kara Seas: *GEOLOGIYA I GEOFIZIKA*, v. 43, no. 11, p. 1049-1052.
- Vågnes, E., and Amundsen, H. E. F., 1993, Late Cenozoic uplift and volcanism on Spitsbergen: Caused by mantle convection?: *Geology*, v. 21, no. 3, p. 251-254.
- Weinbruch, S., Drotikova, T., Benker, N., and Kallenborn, R., 2015, Particulate and gaseous emissions of power generation at Svalbard (AtmoPart): Governor of Svalbard, Svalbard Environmental Protection Fund.
- Yuan, Y., Zhu, W., Mi, L., Zhang, G., Hu, S., and He, L., 2009, “Uniform geothermal gradient” and heat flow in the Qiongdongnan and Pearl River Mouth Basins of the South China Sea: *Marine and Petroleum Geology*, v. 26, no. 7, p. 1152-1162.
- Zhuo, Q., Meng, F., Zhao, M., Li, Y., Lu, X., and Ni, P., 2016, The salt chimney effect: delay of thermal evolution of deep hydrocarbon source rocks due to high thermal conductivity of evaporites: *Geofluids*, v. 16, no. 3, p. 440-451.